2. Project context and objectives

When dealing with cancer and other serious illnesses any improvement in the efficacy and availability of proper diagnostic procedures turns out into a benefit for the patients. Early diagnosis reduces mortality and increases not only the success probability of a therapy, but also the quality of life of the successfully treated patients. It may also have beneficial effects on minimising the high therapy costs. Diagnosis that provides information about

- three-dimensional regional distribution of the cancer and of its functional activity
- three-dimensional functional imaging of other illnesses
- type and staging of the disease to be treated in each specific case
- outcome of the therapy

is therefore very important.

Three-dimensional (3D) functional nuclear medicine imaging satisfies the above requirements. Especially the combination of today's PET and SPECT systems with CT scanners allows simultaneous acquisition of anatomical and functional information within one single diagnostic session, and this results in a more precise combination of the complementary information as well as in a reduced inconvenience for the patient. The use of these imaging procedures, which are based on the detection of radiation emitted by (or traversing/scattered from) the patient is however associated with a sometime significant radiation exposure of the patient. The introduction and continuous development of new diagnostic procedures based on CT, PET and SPECT imaging resulted thus in the last years in a rapid growth of the individual dose caused by medical exposures. The minimization of the dose to the patient is unfortunately often still considered a second-order problem, as image quality, and velocity and easiness of the examination are generally the criteria leading to the introduction of new procedures. The radiation protection issue is highly topical also for nuclear medical diagnosis, since in this case radiopharmaceuticals are administered to the patient, meaning not only a radiation exposure to the presumably cancerous tissue but also to the surrounding healthy tissues and to the other organs where the administered radioactive agent is distributed and deposited.

Aim of the MADEIRA project was to improve the efficacy and safety of 3D functional imaging by optimising the spatial resolution, the signal-to-noise ratio and the knowledge of the temporal variation of the radiopharmaceuticals' uptake in and clearance from tumour and healthy tissues. Specifically, it was intended to:

- develop a specific detector array system (magnifier probe) to be used as an add-on to conventional PET or PET/CT devices;
- develop and optimise two physics-based image processing tools for noise reduction and for image reconstruction and adapt them to nuclear medicine imaging;
- develop new time schemes for application and imaging of radiopharmaceuticals using pharmacokinetic modelling techniques;
- improve dose assessment by combination of realistic pharmacokinetic models to calculate activity distribution in the body and anthropomorphic voxel phantoms to calculate energy deposition in the tissues.

The approach developed in the frame of the Project will enable to guarantee or even improve the quality of the diagnostic information reducing the amount of administered activity, i.e. reducing the exposure to ionizing radiation and specifically the dose to the healthy tissues of the patient.

3. Main S&T results

The scientific work was subdivided into four work packages:

WP1 - **Assessment of clinical data**, coordinated by Malmö University Hospital/Lund University;

WP2 - **PET magnifier probe development**, coordinated by Jožef Stefan Institute;

WP3 - **Physics-based image processing**, coordinated by Helmholtz Zentrum München;

WP4 - **Biokinetic and dosimetric modelling**, coordinated by Università degli Studi di Milano.

The general goal of the project of improving safety and efficacy of nuclear medicine diagnostic applications by minimizing patients' exposure was pursued following three paths:

1. improvement of the imaging process by means of the development of a novel detection system (made in Workpackage 2),
2. improvement of the imaging process by means of the development of new algorithms for noise reduction and image reconstruction (Workpackages 1 and 3)
3. improvement of biokinetic and dosimetric estimates by means of a more realistic description of the biodistribution of the radiopharmaceuticals and of the internal dose deposition patterns (Workpackages 1 and 4).

3.1 Development of a novel detection system

The approach chosen for improving spatial resolution and detection efficiency in PET imaging was that of developing a so-called PET imaging probe, to be used as an add-on to conventional PET or PET/CT devices. The rationale behind this idea is shown in Figure 1.
The probe is a partial detector ring which is designed to be inserted within a standard PET unit and to be placed close to the imaged object, so to have a large field of view of it. Events collected in the probe will have high spatial resolution information. High-resolution events will be combined with data collected by the external (conventional) PET ring, the data from external ring serving to remove artefacts due to limited angle tomography. Adding data with high spatial resolution improves the quality of image for a given dose or, conversely, reduces patient dose for a given image quality.
In the development of the system new technological solutions regarding packaging, detection and signal acquisition systems were looked for. Not all of these technological aspects could be fully investigated due to problems encountered with the production and supply of read-out chips. These problems required the efforts of the research groups to be mainly focussed on the development and testing of the chips. The development of alternative technological solutions for optimized hardware could therefore be pursued only with reduced intensity and was considered as a fall-forward option.

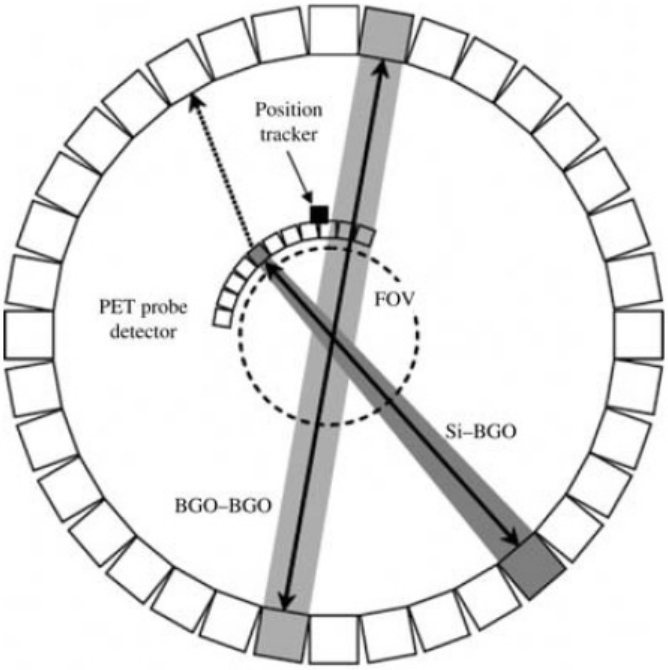

Figure 1. Schematic representation of the PET probe inserted in a conventional PET ring. The full arrows indicate the possible ring-ring or ring-probe coincidences, the dotted arrow indicates a scattered photon. The shaded areas represent the position uncertainty.

Detectors

High-resistivity silicon was chosen for probe material for several reasons: (i) excellent spatial resolution of segmented detectors, providing means for proximity focus exploitation; (ii) compactness and sturdiness, simplifying mechanical design; (iii) developed design and processing technology; (iv) good energy resolution, enabling event classification and Compton scatter recognition; and (v) possibility of operation in magnetic field. The most serious drawback is its low efficiency; only 2 % of incident annihilation photons interact in 1 mm thick silicon, with Compton scattering being the most common interaction. On the other side, more sensitive materials exhibiting higher efficiency, like scintillators coupled with light detectors, have serious limitations when aiming for compact systems with high spatial resolution.

The resolution requirements for the PET Probe were discussed at the beginning of the project. It was assumed that even in case of ^{18}F-labelled radiopharmaceuticals an average range of the movement of the positrons leads to an uncertainty of about 0.7 mm at the minimum. Scatter radiation will further reduce the physically achievable resolution. Modelling of the maximum achievable FWHM of the overall system (including the probe) was performed, showing that, for the interesting cases of distances of the probe to the localisation of the object in the range of up to 10 cm, it would be possible to achieve resolutions in the range of up to the same FWHM as the nominal pixel size of the probe detector or even a little less. This showed that it would be meaningful to consider pixel sizes of down to 1 mm for the probe detector.

The sensors selected for the pre-clinical PET-probe are therefore 1 mm thick silicon detectors segmented into 1040 square pads of 1 mm side. Such pad dimensions are manageable in terms of module construction, provide sufficient coverage (40 mm x 26 mm) for a sensible probe field of view and are stackable to achieve efficiency up to ~10 % for 511 keV photons.

A stock of such detectors, produced by SINTEF in double metal layer technology was evaluated using a detector testing system based on a custom 5x5 probe card and built in Ljubljana. Measurements of full depletion voltage, inter-pad resistances and leakage current for all pads of the detectors have been performed. Typical leakage current at 500 V bias voltage was found to be around 0.2 nA per 9 pads, well below the maximum acceptable value. Six 1040 pad detectors proved to be suitable for construction of a probe prototype using wire-bonding technology.

Front-end chips

The VATAGP7 ASICs (application-specific integrated circuit), produced by GammaMedica IDEAS (GMI) in Norway, were chosen, since their specifications are matched well to the probe

needs. The shaping time of the fast shaper was shortened to 45 ns to reduce time-walk without increasing excessively the jitter. Further improvements were possible due to the technology change, moving from the obsolete 0.8 µm to 0.35 µm triple-metal AMS process.
Unfortunately, upon initial testing of the digital functionality of the chips, a serious error was discovered. This error caused the address of the triggered channel to be disabled, thus making the chips useless for any high-rate application. The error was traced back to an erroneous connection in the first metal layer. A temporary solution for the problem, focused ion beam (FIB) treatment for cutting the redundant line, provided a stock of chips suitable for prototype work until resubmission. Due to internal problems at GMI the resubmission was delayed by 6 months, resulting in delivery of the new chips at the end of September 2009, 16 months after the failed first run.
After delivery of the new chips most of the resources of the groups involved in WP2 were focused into evaluation of the chip performance. The chips from the resubmission run were found to be fully operational and their specifications well matched to the probe needs. Immediately after the evaluation the chips were used for construction of double-sided module using 512 pad detectors as level zero prototype. This work demanded an extra effort from all the research groups involved, and thus limited the possibility to follow more effectively the development of other features of the probe, in particular the packaging technology (see below). Anyway, even with a significant delay with respect to the original timeline, it was possible to obtain a sufficient stock of fully functional front-end chips to produce the probe prototype in time for testing.

Packaging technology
A crucial aspect for the assembly of the probe is represented by the packaging technology. Different concepts of packaging were investigated. The first is the well proven wire–bonding of the pads, routed to the detector edge via a second metal layer on the sensor, to the read-out chip. For that purpose custom pitch-adapters (1 µm Al on 300 µm glass) were designed and submitted to fabrication at CNM Barcelona. While being a robust technology, well mastered by the consortium, wire-bonding allows a modest filling factor of ~30 % when stacking multiple (>2) layers of silicon sensors.
In the chosen approach detector pads are routed via second metal layer to the detector edge. Custom made pitch adapters (1 µm Al on 300 µm glass) were developed to fan-in the lines from detector pitch to the front-end chip pitch (see Figure 2a). Wire-bonding was used to provide connection from the detector to the pitch adapter as well as from the pitch adapter to the front-end chips. This robust technology, well mastered by the consortium, was used in the construction of four detector modules without major problems Alternative mechanical configurations (described below) were devised in order to reach the desired filling factor of about 70%.
Two other packaging technologies, with better performances with regard to the achievable filling factors, have been investigated: Tape Automated Bonding (TAB) and fine pitch multilayer flexible printed circuit (FPC). Due to the problems related with the front-end chips, the resources dedicated to the studies on these technologies had to be reduced; therefore the PET probe prototype finally produced and tested at the University of Michigan was still using the wire bonding technology.
Even if not fully developed for a routine utilization for the probe prototype, the two technologies of TAB and FPC were anyway further studied.
The TAB technology, which is suitable for bonding electronic circuits on flexible materials like polyimide that can be bent up to 180º, was tested with the module shown in Figure 2b. The module is composed of a 1 mm thick silicon pad detector with 1mm x 1mm pads, and two readout VATAGP3_1 chips from GammaMedica-IDEAS (GMI). The connection of the detector module to the readout electronics was done by means of two cables. One of them covered the detector, and was connected to each of the detector pads from the top. The readout lines went to the edge of the cable, where they were connected to a second cable, which in turn was connected to the ASICs. A flexible structure served as a support for the components and for electric contacts.

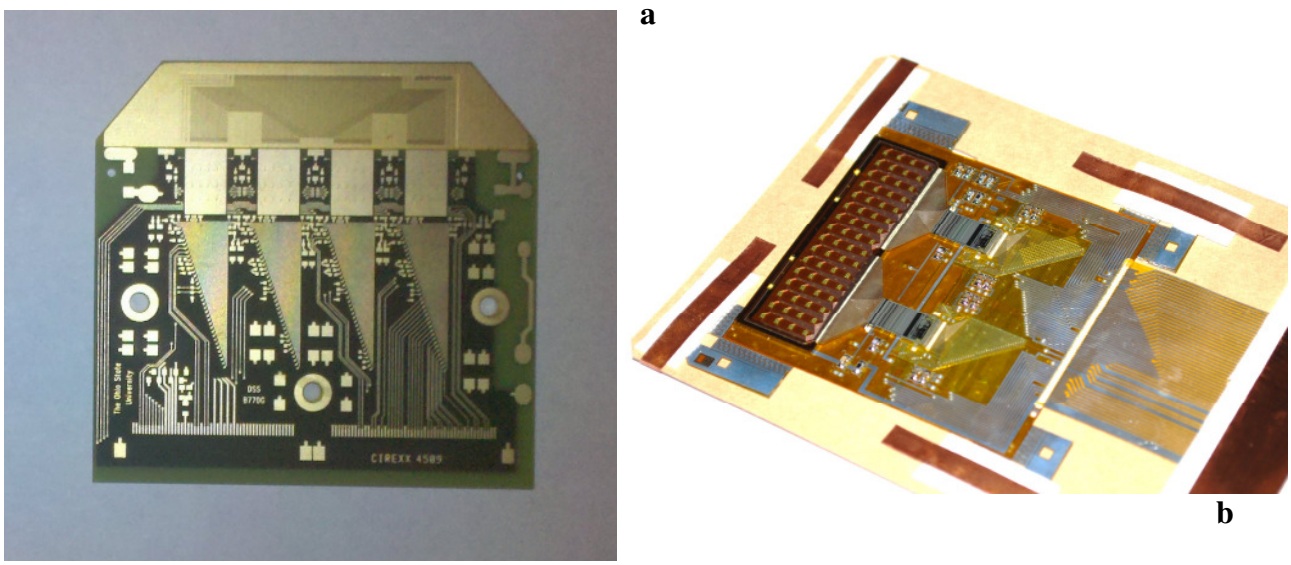

Figure 2. a: Photo of a 4-chip hybrid for 1040 pad detector modules. A pitch adapter can be seen on the top. b: TAB silicon module, composed of a silicon detector connected to the ASICs by means of TAB bonded microcables.

The system was fully operational, and the spectroscopic resolution obtained was comparable to that obtained with wire-bonded modules, demonstrating that the micro-cable technology does not degrade the performance of detector modules. However, some technical problems encountered during the module operation could be solved only near the end of the project, therefore this technology could not be readily applicable to the construction of the first probe prototype.
Significant progress was achieved also with the FPC approach. A geometry suitable for connection of 1040 pad detectors was adopted, based on a rigid central part glued to the detector combined to flexible side parts that allow fanning out to the read-out hybrids where lines are to be wire-bonded to read-out chips. Problems associated with production of four layer fine pitch Cu/Kapton laminates were solved and fully functional cables with 100 µm line pitch were produced. Bonding of multilayer boards to aluminised silicon with thermoplastic adhesive has been performed and initial typical resistances in the range of 10 Ohms were measured. Detector was mounted on flex circuit and 10 channels were readout with charge sensitive amplifier. Signals generated with ^{22}Na source were successfully readout. Accelerated ageing to verify long-term stability showed however increasing resistance of contacts to aluminium surface indicating that underbump metallisation of detectors with other metal (for example gold) is needed. The benefits that will derive from this technology, once it has been fully developed, include the possibility of parallel readout of two sensors, providing either double sensitivity at the same detector thickness or improved timing and constant sensitivity using thinner detectors.

Data acquisition system (MADDAQ Board)
The first test board of the MADEIRA data acquisition system (MADDAQ) was tested in the first week of February 2010 (Figure 3), and a total of 20 boards were then produced for the probe. The implementation of the MADDAQ boards has provided a tremendous gain in term of compactness of the system. Each board can handle one of the MADEIRA probe modules, that comprise two silicon detectors and four hybrids, each hybrid with four VATAGP7 chips. The board layout is composed of 12 layers: 6 routing layers, 4 power planes, and 2 GND planes.
The board operation is controlled by a FPGA Spartan-3 from Xilinx, and a fast communication with the computer is possible by means of an Ethernet connection that can work at up to 1 Gbps. The digitization of the data is done through eight 12-bit ADCs that can work up to 40 MHz sampling rate. A series of programmable DACs will allow setting the required biases for the ASICs.
The custom firmware was developed in parallel to the DAQ system

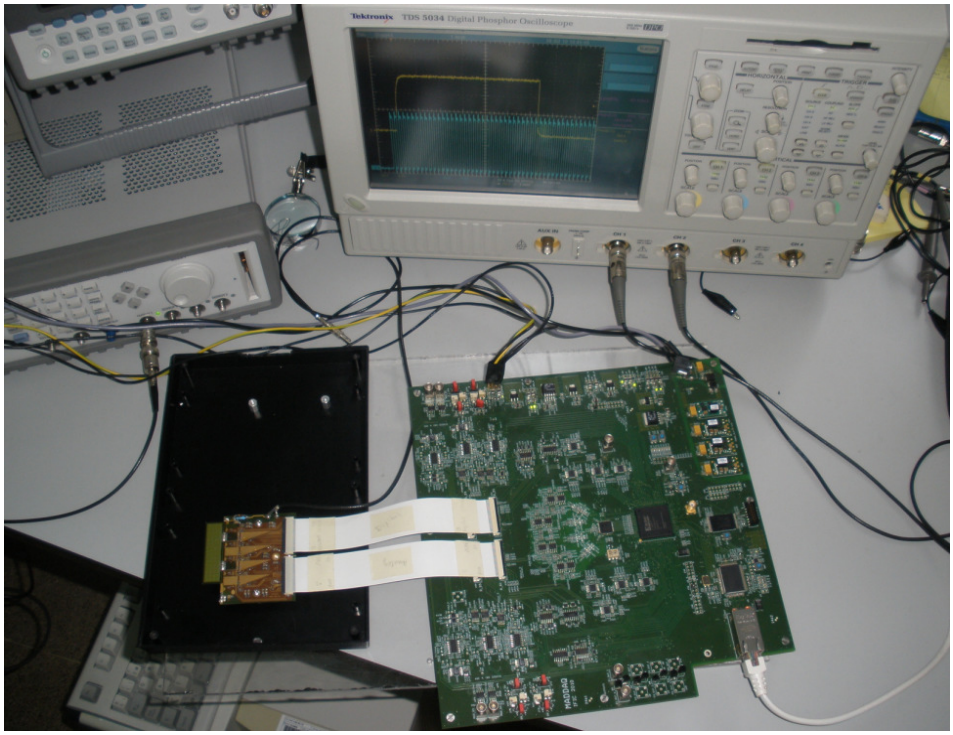

Figure 3. First MADDAQ acquisition system connected to a probe hybrid.

PET probe prototype

As a consequence of the problems experienced with the front-end chips, prelinminary tests of the probe prototypes were made with two smaller evaluation modules, using the same ASIC type, hybrid and electronics, but with FIB-ed GP7 chips, 1 mm sensors with 256 square pads of 1.4 mm side, and consequently only 2 VATAGP7s. The evaluation module was tested and the observed energy resolution of 1.5 keV FWHM proved that the performance of the probe fully complied with the requirements. The comparators could be calibrated and aligned to within 1 keV peak-to-peak variation and timing performance was proven to be well understood. This allows operation at timing windows down to 20 ns. The measured characteristics confirmed the validity of the selected approach.

A level zero prototype module, consisting of two 512 pad sensors (1 mm thick square pads with a side of 1.4 mm), glued back to back to an 8-chip (4 per detector) double-sided hybrid, was then built as soon as the resubmitted chips had been positively evaluated. The module was successfully tested. The fit of the photopeak in the spectrum obtained by ^{241}Am source tests (Figure 4) gives an energy resolution (FWHM) of 2.5 keV. The reduced resolution as compared to 256 pad module is an expected consequence of increased number of read-out chips. It is however well within the the requirements for the probe. The measured energy resolution is not expected to vary significantly with increasing energy (up to 511 keV) as it is dominated by electronics.

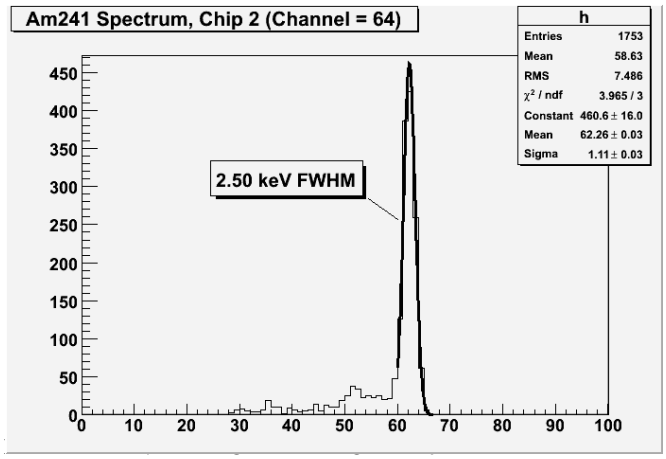

Figure 4. Spectrum obtained by ^{241}Am source tests of the double-sided module with 512 pad detectors for level zero prototype.

The next step was production of double-sided modules (2 sensors per module) using 1040 pad sensors (1 mm thick) with 1 mm square pads wire-bonded to two double-sided hybrid boards each carrying 8 VATAGP7 read-out chips. (Figure 5).

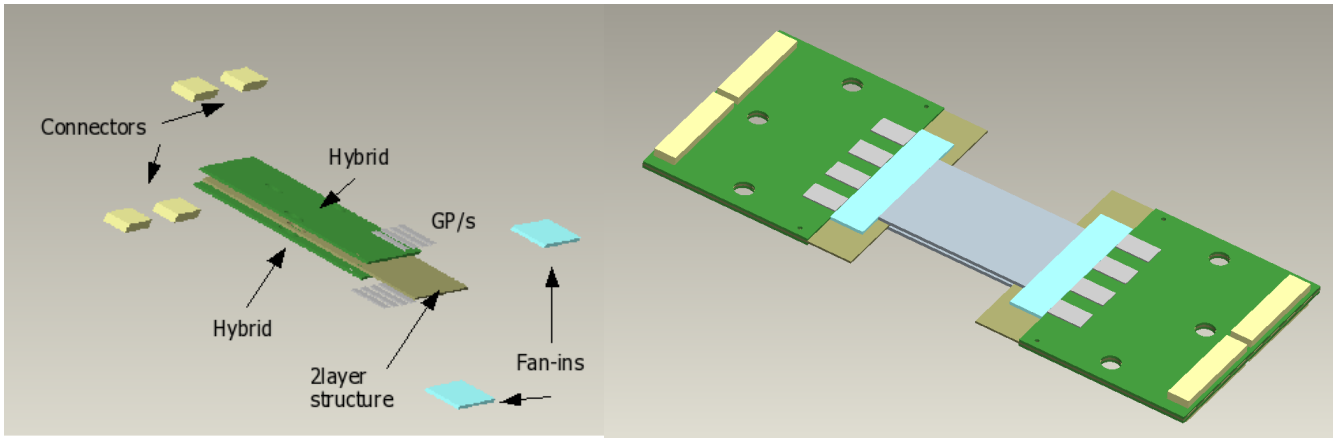

Figure 5. Mechanical design of a double-sided detector module.

Each module was built with 2 hybrids placed on each side of a pair of 1 mm thick silicon sensors, each hybrid containing connectors, flexible boards, support structure, ASICs and pitch adapters. Modules can be assembled together to build a probe stack with either both modules parallel to each other or orthogonal to each other (Figure 6). The parallel approach provides full sensor overlap but has a lower filling factor (around 30%), while the orthogonal option provides a significantly higher filling factor (up to 70%) at a cost of reduced sensor overlap, thus reducing efficiency of the system. The chosen mechanical design is flexible enough to try both options easily and study the benefits of each one.

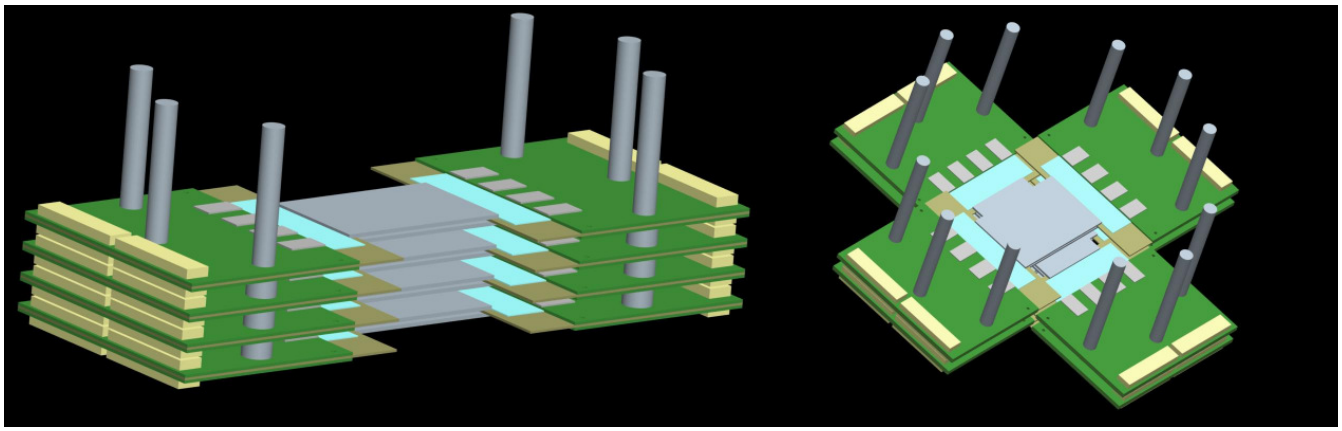

Figure 6. Designs of a probe stack with the modules in parallel (left) and orthogonal (right) configuration.

The first module of the probe was assembled in April 2010. The second module of the final PET probe was assembled in September (Figure 7). The modules were characterised, exhibiting energy resolution around 2 keV FWHM, stable operating thresholds of 20 keV and negligible number of unusable channels. A versatile mechanical support structure allowing for different probe module configurations was designed and fabricated.
Collection of first images was started in July 2010 at the University of Michigan, Ann Arbor. The setup consisted of 24 refurbished BGO blocks from an old clinical PET scanner (crystal size of 6 x 13 mm2) arranged in a partial ring of two arcs each covering 67.5° at a radius of 52 cm. Initially two level zero probe modules were placed inside the ring at a distance of 6.5 cm from the centre. To limit the accidental rate and increase efficiency the probes were arranged in an edge-on geometry

behind a 1.5 mm slit. Such an arrangement (shown in Figure 8) allows collection of three types of PET events. In order of increasing resolution: ring-ring (yellow line), ring-probe (red line) and probe-probe (green line).

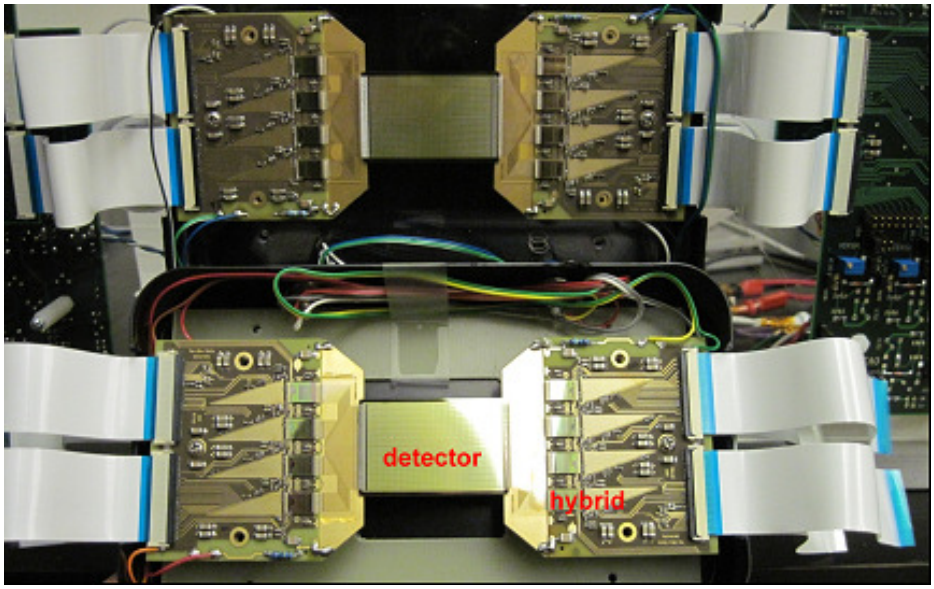

Figure 7. Two final probe modules on a test stand. Each module contains two silicon detectors and four hybrids.

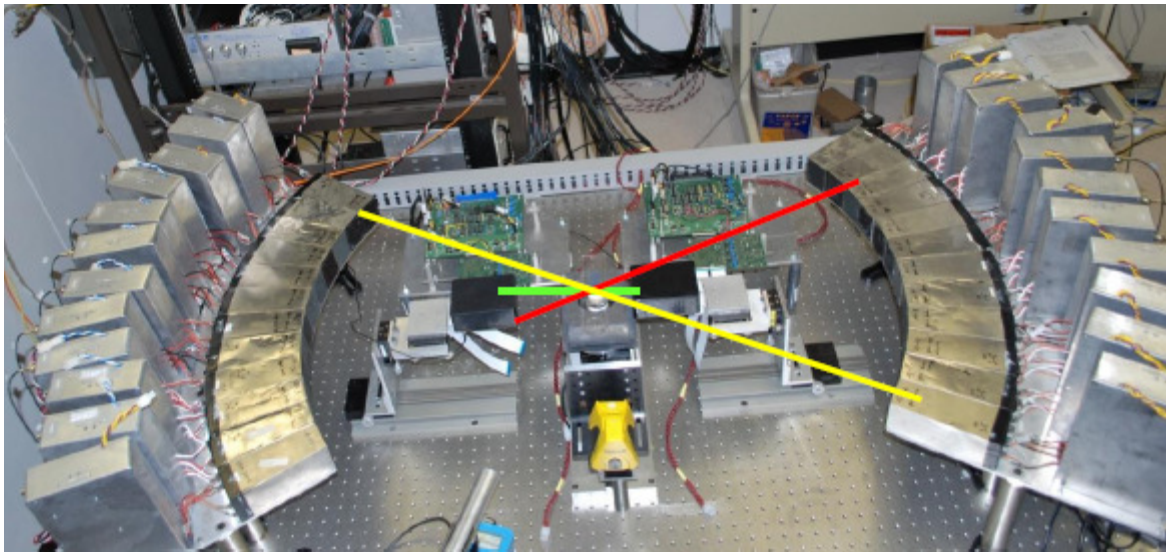

Figure 8. The arrangement for the testing of the probe modules inside the clinical PET scanner at the University of Michigan, Ann Arbor.

The imaged objects include ^{22}Na point sources as well as hot and cold Derenzo phantoms filled with ^{18}F. The objects were rotated by 360^{o} and data were taken in 60 angular views. Filtered back projection (FBP) followed by ML-EM iterative reconstruction were used to evaluate performance of the system.

Results showed that already at FBP level three point sources placed 2 mm apart can be clearly resolved in images reconstructed from either probe-probe or probe-ring dataset. Reconstruction of Derenzo phantom images exhibits comparable feature recognition performance from probe-ring and probe-probe datasets (Figure 9). This proves the concept of the PET probe; even in case of an out-

dated, "low-resolution" imaging system an addition of high-resolution data from the probe improves resolution of the combined system to the intrinsic resolution probe.

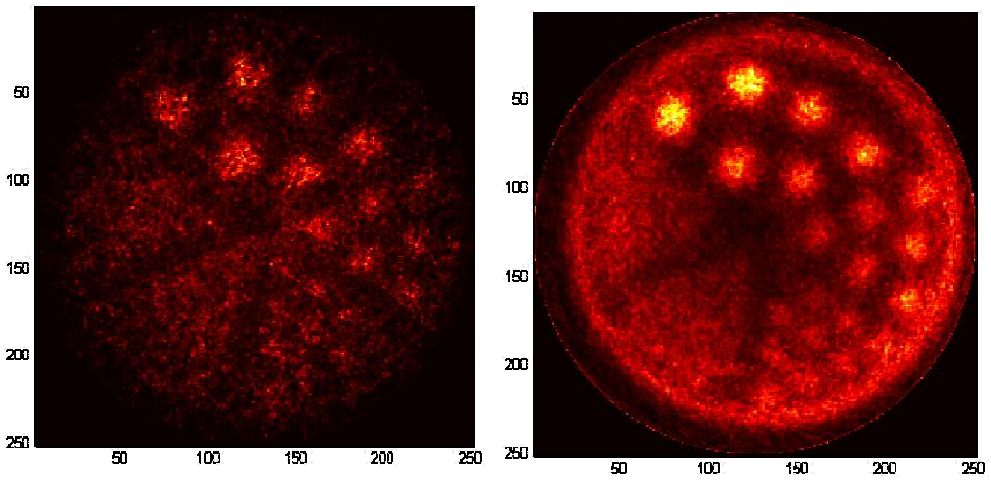

Figure 9. Simultaneous images of a hot Derenzo phantom based on probe-probe (left) and probe-ring (right) datasets.

In additional to the experimental measurements, an ideal system simulation and image reconstruction study has been performed in order to assess the potential improvement in image resolution offered by the probe in a clinical PET system. The model includes a probe consisting of ten layers of silicon spaced 2 mm, each being a 80x52 array of 1x1x1 mm^3 pixels, in coincidence with a PET scanner modelled on the Siemens Biograph 64. The system was modelled using GATE. Simulations were run with various activity distributions including a Derenzo phantom.
Images have been reconstructed with the ML-EM algorithm. The Siddon ray-tracing algorithm was used to compute both the system matrix elements (on the fly) and the sensitivity image for the different types of datasets: conventional PET coincidences and probe-ring coincidences. An examination of images reconstructed using the probe-ring data only shows an improvement of spatial resolution in an area close to the probe when compared with the PET images. The full-width half-maximum of the point-spread function was found to be halved. A joint reconstruction algorithm, employing multiple Siddon line-elements, was developed to assess the two data components simultaneously. Oversampling allowed the coarse resolution data and the fan-like probe-ring response to be accurately described. The new system matrix was utilized in the on-the-fly list-mode ML-EM algorithm using all data (ring-ring and probe-ring) simulated.

3.2 Development of new algorithms for noise reduction and image reconstruction

New algorithms and approaches were developed and then tested using images obtained from experimental measurements with phantoms or directly clinical images of patients.
Part of the work was facilitated by the software platform “scientific visualizer” developed by Scivis. This platform decouples different tasks:

- Input/Output (Dicom and proprietary nuclear medicine image formats);
- Processing of the loaded data set (OPED, ReSPECT, other);
- Visualization of result;
- Postprocessing of result.

Due to decoupling, the versatility of the platform for project purposes was greatly enhanced, as different processing blocks could easily be integrated as plugins and the visualization part of the software served as a common standard amongst the project partners. In this way frequent misconceptions, due to the use of different platforms (with different interpolation schemes at different magnification levels, different compression of color bars, etc.) were circumvented.
In the course of the study the need of a specific phantom for evaluation of spatial resolution in PET and SPECT imaging was acknowledged. An ad-hoc phantom was therefore devised ("MADEIRA phantom") and a patent application for it has been filed. Another patent was filed for a new reconstruction method developed by the project.

New algorithms for image reconstruction and noise reduction

In nuclear medicine imaging the geometrical and statistical parameters are different compared to diagnostic radiology meaning that the methods to be tested against other reconstruction methods in nuclear medicine are to be adjusted to the imaging process, and that standardization for the evaluation process is necessary.
Scivis and HMGU were able to build a completely new image reconstruction method for nuclear medical imaging. This is based on the compressed sensing (CS) paradigm which allows for reconstructing data from very few measurements, provided the object is (in a mathematical sense) "sparse" or "compressible". The mathematical theory behind this strategy, as known so far, was however not able to deal with Poissonian noise which is characteristic of nuclear medicine imaging. We have been able to adapt the complex theory to Poissonian noise and can thus reduce the number of measurements considerably while retaining the same image quality. The methodology was filed as a patent application on January 28, 2010.
The structure-saving non-linear noise reduction algorithm developed by the project coordinator and others and patented by the HMGU (patent filed in 2003) was adapted to the nuclear medicine case (SPECT). This adaption was not straightforward, considering that the algorithm had been originally devised for reducing anatomical noise and statistical (i.e. mostly quantum) noise in projectional radiography and implemented into the scheme of CT investigations. It was necessary therefore to find optimal adaptive relocations to correct for the different imaging geometries typical of nuclear medical imaging, in particular the high statistical noise. A module was developed to estimate possible signal-to-noise levels for application of the proposed non-linear noise reduction technique.
The adaption to SPECT imaging was possible considering that in the SPECT instrument used in the MADEIRA investigations the two detectors are fixed at 180° to each other and each of it can cover the whole 360° scanning field by rotation. Therefore, two datasets for correlation are available. However, the fact that the position of the emitting radioiosotope is not always centered with respect to rotation axis of the detectors required a solution to take this shift into account. The depositioning implies indeed some time delay in the signal collection of the two detectors, and consequently a rotation phase shift had to be introduced for the data to be correlated.
In addition a similar but even easier approach to reduce artefacts and the related noise in PET images was developed by reconstructing two complementary data sets which are then added together. With this procedure, undersampling artefacts are avoided. This is demonstrated in Figure 10.
All algorithms developed so far within the project have been developed as software codes. These software codes have already been implemented into the software platform "scientific visualizer" provided by Scivis GmbH. This "scientific visualizer", not yet in product status but in a pre-commercial version, was provided with all its components to the project partners for testing the potential advantages of the proposed methods. Currently different of the approaches developed in the project are in a pre-release phase. After fulfilling the regulatory compliances for medical devices (risk-management, handbooks, validation), they will be made commercially available by Scivis in fall 2011. The software codes will be commercialized as generic and task-dependent

medical software solutions. In order to handle this broad variety of different medical software packages economically, Scivis has to implement a quality management system according to ISO 13485 that allows certification for each of those solutions according to Annex II of the Medical device directive EWG 93/42.

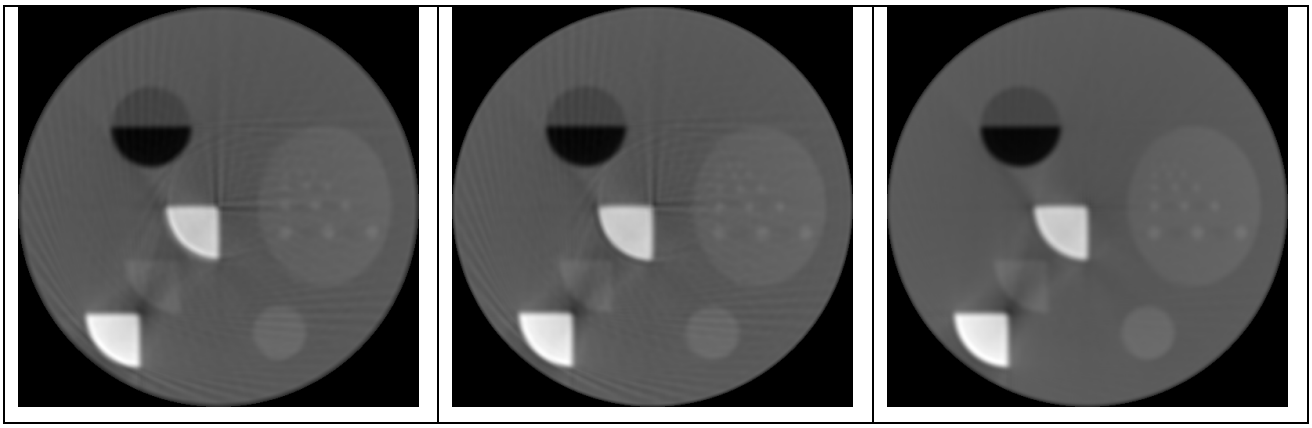

Figure 10. shows a reconstruction of a phantom slice as it is done according to standard sampling schemes in a) and b). However, these two different sampling schemes are supplementary to each other and can be gathered in a single acquisition. In the standard reconstruction this would still produce the same artefacts as seen here. The summation of the reconstructions of the complementary data sets is shown in part c) of the figure. The aliasing artefacts are destroyed due to the principal accuracy of the OPED algorithm.

Experimental tests of image reconstruction and noise reduction softwares

In order to test the softwares developed, a method was implemented for visually assessing the images by showing eight differently reconstructed images to nuclear medicine physicians, who had to grade the three best. Two different tools have been tested, ViewDEX (developed within the CEC-project RADIUS, FIGM-CT-2000-0036) and the "scientific visualizer". ViewDEX proved however not to be yet fully developed for nuclear medicine applications. Discussions with Scivis concerning their "scientific visualizer" platform led to suggestions for adding some features to be used for the observer study. The Visualizer has therefore been implemented according to the suggestions of the physicians of the Nuclear Medicine Department of Skåne University Hospital, and successively nuclear medicine physicians assessed the images reconstructed with Flash 3D. This study could be fully performed only in the last semester of the project due to this optimisation process.

A number of measurements with a Jaszczak phantom (Data Spectrum Corporation, Model # 5000) were performed to study how different reconstruction parameters influence the image quality, in particular to find the optimal number of subsets and iterations required to be used. In addition to the phantom images, also raw data for 18 patients suffering from neuroblastoma or pheochromocytoma and investigated with ^{123}I-metaiodobenzylguanidine (MIBG) have been collected. Images have been reconstructed for different equivalent number of iterations (defined as the number of subsets times the number of iterations), using the Siemens iterative algorithm Flash 3D. The algorithms ReSPECT (iterative) and OPED (analytic), made available in the frame of the project, have been adapted for ^{123}I-MIBG examinations and implemented in the "scientific visualizer" platform from Scivis.

The new noise reduction methods developed in the MADEIRA project and made available to use in combination with OPED have also been implemented in ReSPECT. Denoised patient images have been reconstructed with ReSPECT and OPED. Some problems were originally experienced with OPED reconstruction, whereas ReSPECT could not handle 2 times 360° imaging with two detectors but these problems could be resolved within the project duration.

MADEIRA phantom

In the course of the project the need for a specific phantom for the characterization of PET and SPECT systems was acknowledged. This led to the creation of the "MADEIRA phantom". A preliminary version of the phantom was already developed in 2009 (see Fig. 11, left). It consisted of twenty-one cones with separate valves for filling with radioactive solution. The cones were placed within a half-cylindrical surrounding vessel which is also fillable with radioactive solution for simulating a low activity background.

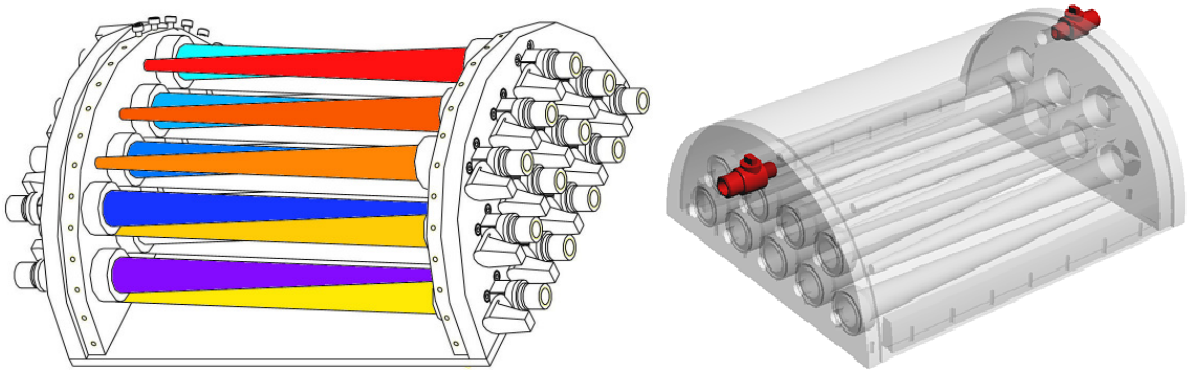

Figure 11. The MADEIRA phantom. Left: first design; right: final design.

The phantom was developed in cooperation with the clinical partner (ULUND) and was designed to specifically fit into the RSD Alderson thorax phantom, so that it could be used for a standardized testing in a clinically relevant situation.

Preliminary tests highlighted some construction and leakage problems. A second version of the phantom was therefore designed (Figure 11, right) and applied for measurements in a clinical environment. SPECT (^{99m}Tc) and PET (^{18}F) measurements with the redesigned phantom with 16 cones have been performed, with the cones filled with activity levels differing by a factor of 3/4 from one to the other. The lowest relative activity concentration was one tenth of the background activity concentration in the external vessel, and the highest concentration was ten times higher than the background. Eight cones contained activity below background, and 8 cones above background. As a start, one SPECT and one PET measurement were performed with very good statistics. Figure 12 shows representative SPECT and PET images of the new phantom.

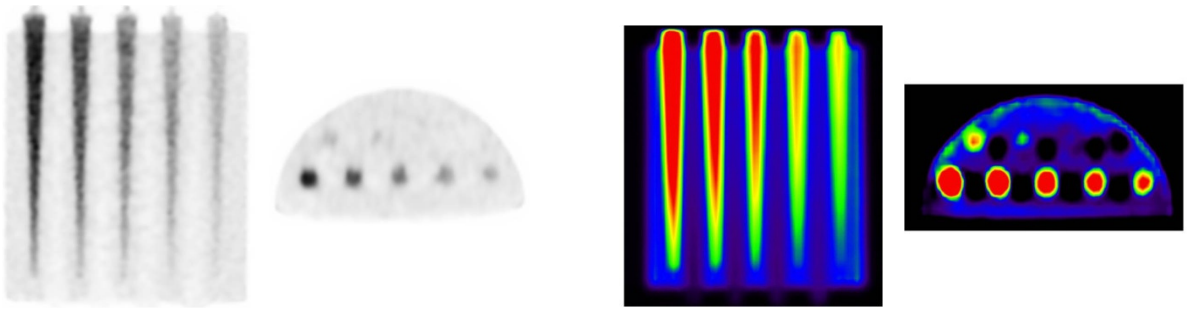

Figure 12. Representative SPECT (left) and PET (right) images of the new phantom.

Figure 13 shows one application of the phantom for evaluation of spatial resolution and, in particular, of the partial volume effect (pVe). pVe is manifested in the underestimation of the activity contained in a region, when the dimension of this region falls below a certain threshold. The

use of a phantom with cones, which change their diameters continuously and not stepwise, is very helpful in finding the dimension of the region when the pVe starts to play a role. Figure 13 shows that this happens when the diameter is about 1 cm or less.

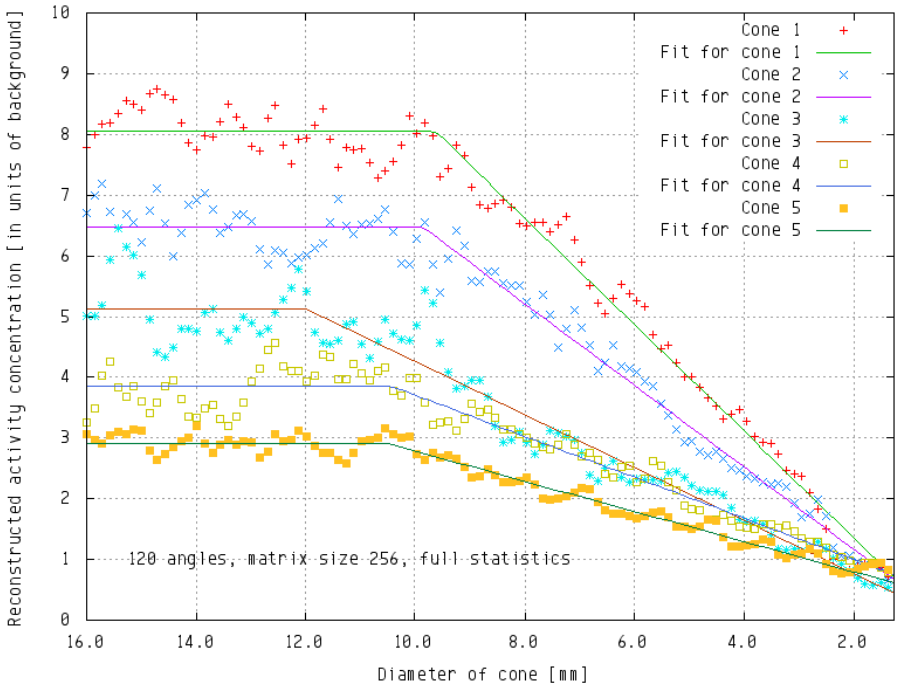

Figure 13. Reconstructed activity concentration as a function of the cone diameter as resulting from the analysis of the SPECT images of Figure 12. The activity concentration was normalized to the background activity concentration, measured in a cone-free area inside the vessel. The cone diameter is linearly related to the distance from the cone base.

Other applications of the phantom include the evaluation of figures of merit such as detectability, signal-to-noise, and resolution depending on the total number of counts and projections and parameters for various reconstructions. In order to do that, further tests were performed by varying the acquisition parameters and the count statistics for the SPECT measurements. By using Monte Carlo simulations, the total number of photons was varied. The number of projection angles was varied by taking only a subset out of the 240 total projections. The matrix size was reduced by rebinning. The phantom proved to be useful for comparison and optimisation of different acquisition and reconstruction parameters in nuclear medicine tomographic studies and for comparisons between various tomographic units.

Figure 14 shows the result obtained in the reconstruction of the MADEIRA phantom. The left panel gives the reconstructed images using the compressed sensing (CS) methodology with only 15 projection angles. Note the smoothness of the hot cones and the detectability of the cold ones. The image in the right panel of figure 13, obtained with standard algorithms from 48 projections, appears slightly less noisy, however the hot cones have jagged edges and the cold cones are hardly discernable at all. Thus it can be clearly stated that CS turns out to be extremely advantageous to reduce to about one third the amount of projections necessary for artifact-free reconstruction, as well as to reduce the necessary activity administered.

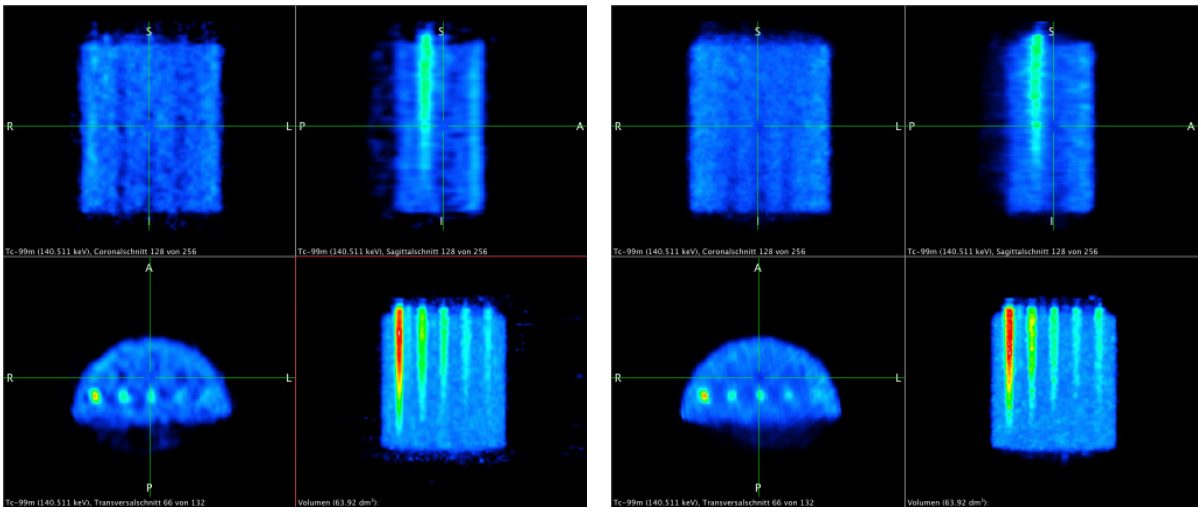

Figure 14. Left: Reconstruction of the MADEIRA phantom from *15 angles with very poor statistics* (23 counts maximum) *using CS*. **Right:** *Conventional penalized likelihood reconstruction* from *48 angles* (more than 3 times the number of angles of the CS reconstruction).

The existing ReSPECT algorithm has been modified in terms of advanced regularization schemes obeying also the characteristics of Poissonian noise. For the first time this allows a marketable product to iterate for an arbitrary number of iterations. As a consequence the free parameters for the iteration process are reduced and more information can be gained from nuclear medicine imaging data sets as it can be visualized for the myocardial perfusion study as shown in Figure 15. The enhanced delineation of the myocard and the better definition of its interior lumen in the image reconstructed with the new scheme can be appreciated.

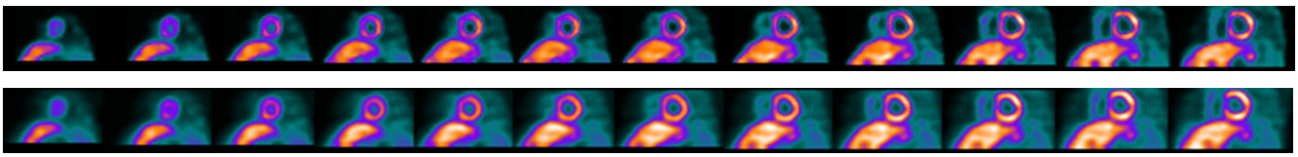

Figure 15. ^{99m}Tc-sestamibi myocardial perfusion study showing reconstructed short axis planes. Above: applying the new regularization schemes and reconstructing virtually with an infinite number of iterations. Below: Common result by prematurely stopping the iterations.

The results have shown that the new schemes work best with non-manipulated measurement data. This is due to the fact that they rely on Poisson statistics of the measurements. The usual methods for reduction of object scatter in measurements however manipulate multispectrally acquired projection data before reconstruction. An alternative strategy that accounts for multispectral scatter data during the iteration itself is conceptually developed. The implementation and verification will be done after the end of the project.

3.3 Improvement of biokinetic and dosimetric estimates

Patients studies have been performed for selected diagnostic applications of radiopharmaceuticals in order to improve the knowledge of the biokinetics of the administered substance and consequently to optimize the imaging protocol. The results of these studies have also been combined with new knowledge on the dose deposition patterns in the internal organs, obtained by application of mathematical voxel phantoms created from tomographic images of real persons. This has enabled to obtain more realistic dose estimates for the diagnostic applications under consideration.

Ethical approval for patients' studies

An application for the conduction of patients' studies was approved on October 30, 2008 by the Regional Ethical Vetting Board at Lund University (Dnr 473/2008). Permission from the ethical committee was received for

1. biokinetics of ^{18}F-choline
2. time optimisation of ^{18}F-choline imaging of prostate tumour and their metastasis
3. biokinetics for ^{123}I-ioflupane
4. time optimisation for ^{123}I-ioflupane
5. respiratory gating for ^{18}F-FDG.

The late approval (10 months after project start) was caused by some complementary work and supplementary information requested by the Board after the original application presented at the beginning of the project. This delay has affected somehow the recruitment of patients so that at the end of the project the number of investigated subjects was less than originally planned. In addition to that, one further major problem of the recruitment of suitable patients for biokinetic investigations with ^{123}I-ioflupane was linked to their illness (Alzheimer's disease), which made them hardly collaborative and required special efforts from the staff. In order to remedy this situation, a contact was established with a member of the research team of Beneficiary 2 (ULUND) at Norrland's University Hospital in Umeå, in view of the high number of ioflupane-patients investigated there. Despite all the efforts and the goodwill of all involved subjects, it was not possible to start patient studies at Umeå Hospital according to the protocol used in Malmö during the project. Nevertheless, the consortium was able to perform all activities as indicated in the work plan and in the list of deliverables.

Respiratory gating

The issue of respiratory gating was investigated in PET/CT studies with ^{18}F-FDG. Breathing during imaging results in blurring of the structures in the images, which is degrading the image quality. This affects the accuracy of quantification and may also result in an overestimation of the lesion volume and obscure the possibility to detect small tumors. The studies on respiratory gating were performed using the equipment supplied by Philips Medical Systems, which is based on a bellows (belt) with Mayo Clinic Respiratory Feedback System. Only specific parts of the breathing cycle, in advance defined, contributes to the information in the CT and PET-image. For each of the five patients investigated, imaging was performed twice, once with respiratory gating and one without.
The results obtained showed that respiratory gating does improve the image quality. However, none of the patients studied showed an uptake in the gated images that were not seen at all in the non-gated.

Quantification of activity in body organs and tissues

A number of measurements on anthropomorphic phantoms was done in order to develop and validate the methodology for quantification of radionuclide content in organs and tissues (including tumour tissues) as well as in the total body of the patients. A cylindrical phantom uniformly filled with ^{18}F-FDG was measured at several time points to verify the response linearity. A cylindrical phantom with hollow spheres of different sizes was filled with different sphere/background ratios to study if the ratios and sphere sizes affects the activity quantification (under this respect, see also the results obtained with the MADEIRA phantom). Comparative quantitative measurements on PET/CT systems from three different manufacturers (Philips in Malmö, Siemens in Gothenburg and GE in Odense) were performed in the frame of an ongoing collaboration between Malmö University Hospital, Odense University Hospital and Sahlgrenska University Hospital. Furthermore, the efficiency of the SPECT/CT camera was studied for ^{123}I to enable quantification of the activity uptake in tumour and normal tissue. In this respect, it was necessary to establish direct links with the vendors of the PET/CT and SPECT/CT units in order to get more detailed information about methods of calculations and image processing than are given to normal clinical users.

In addition, the activity meter for measurements of the injected activity and the gamma counter(s) used for blood and urine samples were calibrated for both ^{18}F and ^{123}I. Samples of different volumes and different activities were measured to find the efficiency (counts per second/Bq) for 511 keV photons (^{18}F) and for 159 keV photons (^{123}I). The same samples were measured regularly over night to study the linearity of the gamma counter and to see at which activity the dead time is low enough for the results to be reliable.

Biokinetics of ^{18}F-choline

Biokinetic studies for ^{18}F-choline administered to patients under screening for suspected recurrence of prostate cancer metastasis started in February 2009. In total 11 patients were enrolled in the study, but for one of them it was not possible to perform the full set of measurements according to the experimental protocol. The protocol included four PET images (thigh to neck) at indicatively 10 minutes, 1, 2 and 3 hours post-administration and collection of blood and urine samples at different post-administration times between the PET scans. Every PET acquisition was preceded by a CT scan, used for attenuation correction and anatomical localisation. In the course of the study the protocol was slightly revised according to suggestions from WP4: instead of taking the first blood sample after the first PET image, i.e. around 30 minutes after injection, the first blood sample was taken before the first PET image, i.e. around 2 minutes after injection.

Figure 16 shows as an example the time-activity curve in plasma (left panel) and the cumulated urinary excretion pattern in the ten available patients.

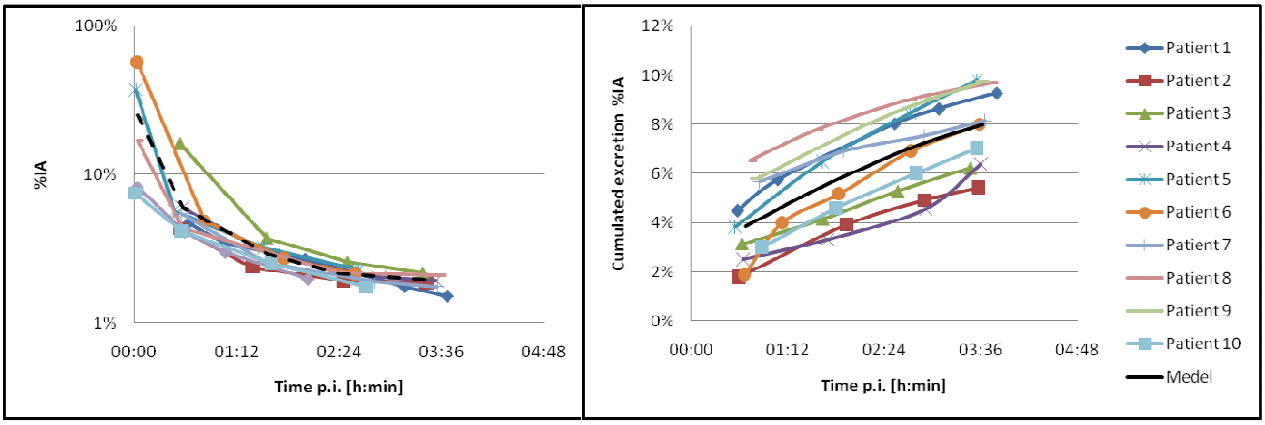

Figure 16. Blood clearance and cumulated urinary excretion after administration of ^{18}F-choline to patients.

Based on these data a biokinetic model for ^{18}F-choline was developed. The starting model was structured as follows: a central exchange compartment, where the injected radiopharmaceutical is initially distributed, and a series of subsystems representing the organs and tissues which concentrated most of the activity and which were easily imaged in all patients: liver, kidneys, spleen and urinary bladder. For some patients activity concentrations were available also for the salivary glands, tumors and/or metastasis. The activities present in these regions were small, so that at this stage of the analysis it was decided not to indicate them explicitly in the general model structure. A further compartment (Rest of the Body, RoB) was added, to account for the material which is transported to organs and tissues different than those explicitly modeled. Identifiability of the compartmental system was verified using the GLOBI software. From preliminary analyses it turned out that the model structure had to be refined to be able to properly describe the experimental data. To this purpose, two alternative approaches were used: (i) the introduction of non-linear kinetics (ii) the definition of substructures using the forcing function approach.

(i) Non-linear kinetics

The introduction of non-linear kinetics was considered because the model overestimated the activity in liver and kidneys, in the first 20 minutes after administration. A process of saturation in liver and kidneys was assumed: after the concentration of choline in these organs has reached a specific

threshold value, the flux entering these organs can't be higher than the flux exiting. Therefore the flux from plasma to liver and from plasma to kidneys has been described using a non-linear equation based on the Michaelis-Menten function used to describe carrier-mediated transport across a membrane. The Michaelis-Menten approach consisted in considering a process of saturation for the transfer rate of ^{18}F-choline from blood to liver and kidneys, respectively.
The results showed that the model can better describe the uptake pattern in liver and kidneys, but at the same time it underestimates the urine data. An alternative approach was therefore followed.
(ii) Forcing function approach
This method allows decoupling a complex multi-compartment model that features a central exchange compartment into several subsystems that are independent of one another. Due to the complexity of the initial model structure and the preliminary results of the non-linear approach, this method was considered more reliable and further developed.
The activity in the central compartment was described with a sum of exponentials with fixed coefficients (forcing function). For each decoupled system, its structure and the parameter values were determined by using the fixed forcing function as an input and fitting the model predictions only to the data collected in that subsystem. The separate substructures were then recombined into the complete model, the forcing function lifted and the new fit performed in the recombined structure. The parameter values obtained in the subsystem analysis were used as starting estimates. Figure 17 gives the structure of the final biokinetic model for ^{18}F-choline biokinetics.

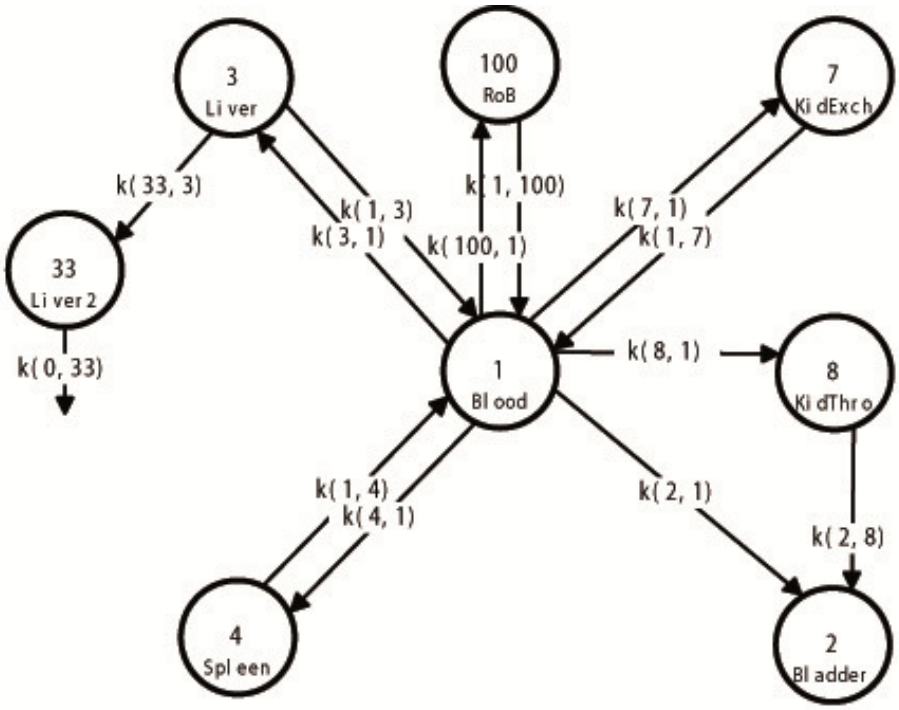

Figure 17. The compartmental structure used for the analysis of the ^{18}F-choline data. ***RoB***: rest of the body; ***KidExch***: Kidney-Exchange; ***Kid-Thro***: Kidney-Through passage.

Table 1 gives the parameter values obtained with the whole set of data in a population kinetics approach (using the software ADAPT). The table lists also the population standard deviation (PSD) and the 99% confidence intervals (CI) of the input parameter values, calculated by adding and subtracting 2.56 times the values of the standard deviation, to and from the mean value. The parameters k(4,3), k(5,1), k(8,1), k(1,7), k(9,8) and volume are assigned to lognormal distributions,

because of their very large uncertainties. For these parameters the assumptions of GSD=1.5 and coverage factor of 3 are made for covering the 99% confidence interval of the data.

Table 1. Values of the model parameters for ^{18}F-choline biokinetics as obtained by the population fit of the model of Figure abc to the available patient data.

Parameter	Mean [min^{-1}]	PSD [min^{-1}]	99% CI [min^{-1}]		Distribution
Blood - Liver1 k(3,1)	$1.61\cdot10^{-2}$	$0.32\cdot10^{-2}$	$7.83\cdot10^{-3}$	$2.44\cdot10^{-2}$	Normal
Liver1 - Blood k(1,3)	$1.84\cdot10^{-2}$	$0.40\cdot10^{-2}$	$8.07\cdot10^{-3}$	$2.87\cdot10^{-2}$	Normal
Liver1 - Liver2 k(33,3)	$2.3\cdot10^{-2}$	$1.7\cdot10^{-2}$	$6.87\cdot10^{-3}$	$7.83\cdot10^{-2}$	Lognormal
Blood - Spleen k(4,1)	$1.13\cdot10^{-3}$	$0.51\cdot10^{-3}$	$3.35\cdot10^{-4}$	$3.81\cdot10^{-3}$	Lognormal
Spleen - Blood k(1,4)	$7.7\cdot10^{-3}$	$2.6\cdot10^{-3}$	$1.07\cdot10^{-3}$	$1.44\cdot10^{-2}$	Normal
Blood - Bladder k(2,1)	$5.1\cdot10^{-4}$	$3.0\cdot10^{-4}$	$1.50\cdot10^{-4}$	$1.71\cdot10^{-3}$	Lognormal
Blood - KidneysExchange k(7,1)	$4.8\cdot10^{-3}$	$1.3\cdot10^{-3}$	$1.56\cdot10^{-3}$	$8.06\cdot10^{-3}$	Normal
KidneysExchange - Blood k(1,7)	$6.2\cdot10^{-3}$	$3.2\cdot10^{-3}$	$1.83\cdot10^{-3}$	$2.08\cdot10^{-2}$	Lognormal
Blood - KidneysThrough k(8,1)	$4.2\cdot10^{-3}$	$1.1\cdot10^{-3}$	$1.33\cdot10^{-3}$	$7.05\cdot10^{-3}$	Normal
KidneysThrough - Bladder k(2,8)	$9.7\cdot10^{-2}$	$2.9\cdot10^{-2}$	$2.28\cdot10^{-2}$	$1.70\cdot10^{-1}$	Normal
Blood - RoB k(100,1)	$6.56\cdot10^{-2}$	$0.91\cdot10^{-2}$	$4.22\cdot10^{-2}$	$8.90\cdot10^{-2}$	Normal
RoB - Blood k(1,100)	$4.6\cdot10^{-3}$	$2.4\cdot10^{-3}$	$1.03\cdot10^{-3}$	$8.25\cdot10^{-3}$	Normal
Volume [ml]	$1.28\cdot10^{4}$	$0.83\cdot10^{4}$	$3.79\cdot10^{3}$	$4.32\cdot10^{4}$	Lognormal

The confidence intervals were used for an uncertainty and sensitivity analysis of the biokinetic model, using a methodology purposely developed in the frame of the project. Latin hypercube sampling and Monte Carlo sampling techniques were used to generate samples that served as model inputs, taking into account the parameter correlations. The most sensitive parameters for selected output and time periods have been identified applying the concept of standardized rank regression coefficient and partial rank correlation coefficient. As an example of the results of this analysis, Figure 18 shows the corresponding 95% confidence interval of the model predictions for Blood, Liver, Spleen, and Kidneys, respectively.

Statistical methods of time series analysis were used to bypass the shortage of experimental data available. These statistical methodologies were used as a complementary integration to the compartmental analysis. In the presence of a significant number of data, these methodologies could represent a valid and faster alternative to reconstruct the data of a single compartment, whether regarding blood, urine or organ data.

Different techniques were developed and applied to the different sets of patient data collected in the ^{18}F-choline studies.

A regressive model was used to reconstruct the blood data, considering the function $F_t = a_0 e^{a_1 t}$, where F_t is the trend, a_0 and a_1 are parameters to be evaluated. The final equation, describing the evolution of the trend of the series considered, was described by the function $F_t = 22\cdot e^{-0.030\cdot t}$.

The smoothing exponential method was used to recover the urine data. The smoothing constant, that satisfies all the constraints (values, sensitivities and limits) and minimizes the Root Mean Square Prediction Error index (RMSPE) was calculated equal to 0.9, and the optimal model to reconstruct the series was described by the equation $p_t = 0.9\cdot X_t + 0.1\cdot p_{t-1}$, where X_t is the value of the series at the time t and p_{t-1} is the value of the prediction at the time t-1.

Finally, the multiplicative moving average method was used to reconstruct the missing data of the bladder organ because, in the experimental data, the size of oscillation varies in proportion to the changes in the level.

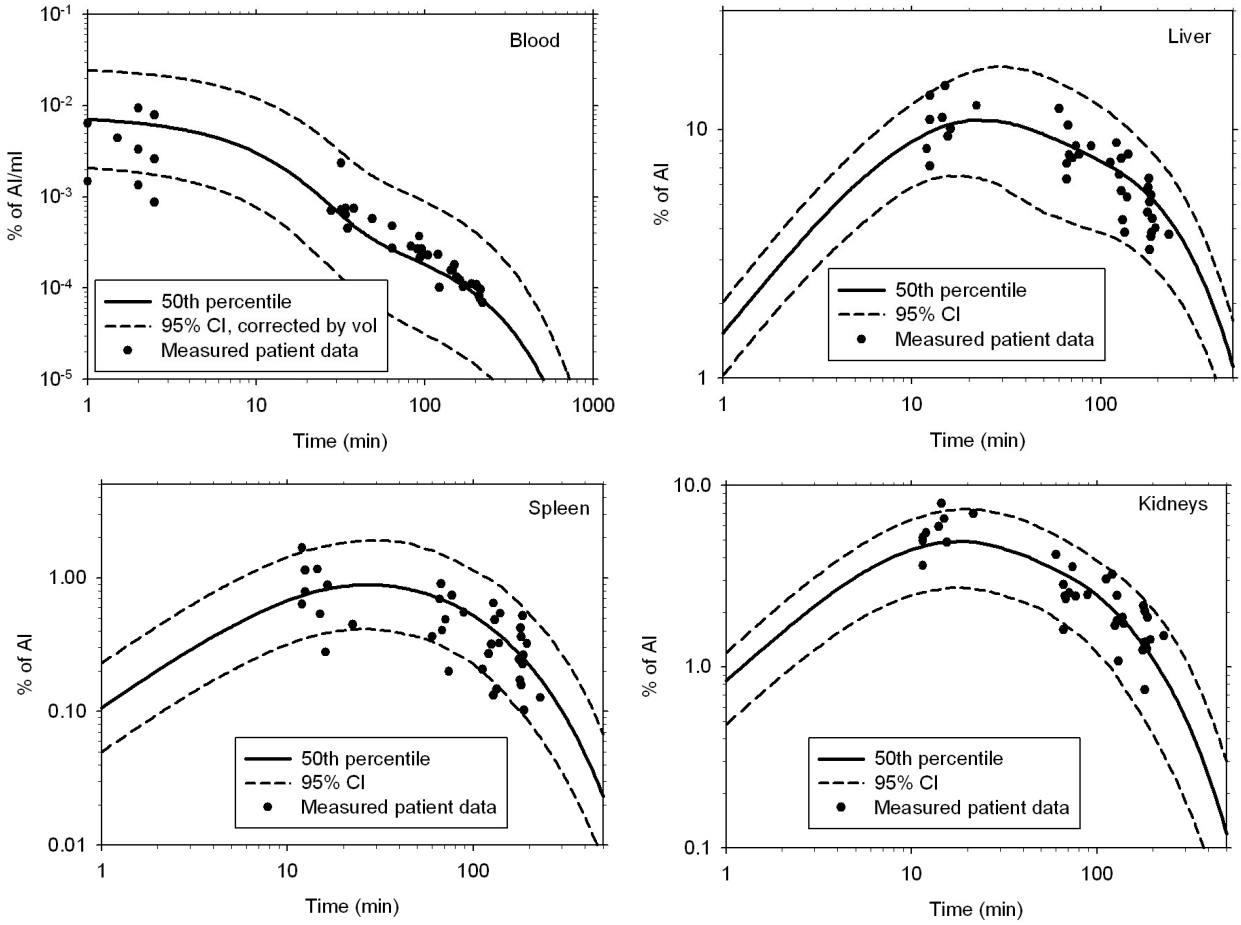

Figure 18. The predictions of the population kinetics model for the compartments Blood (upper left panel), Liver (upper right panel), Spleen (lower left panel) and Kidneys (lower right panel) and the corresponding 95% CI, obtained from the uncertainty analysis. The dots represent the measured patient data.

Biokinetics of ^{123}I-ioflupane (DatScan)

Biokinetic studies in Alzheimer's patients referred to examination with ^{123}I-ioflupane started in late 2009. The experimental protocol consisted in the blocking of the thyroid in the morning (9:00 a.m.), followed one hour later by the administration of 185 MBq ^{123}I. Whole body planar gamma camera measurements were made at the following time points post injection: 10 min, 1 h, 4 h and 24 h. One SPECT/CT scan for biokinetic purposes (quantitative determinations) was performed at 2 h, and one clinical SPECT/CT scan of the brain region was performed at 3 h. Blood samples were collected prior to each whole-body scan, i.e. at approximately 5 min, 1 h, 4 h and 24 h p.i.. All urine was collected from the patients from the time of injection until 24 h p.i. Seven patients were measured and a complete set of biokinetic data was retrieved and analyzed for six patients. Data for the 7th patient consisted only of blood data due to difficulties in managing the patient.

Activity content in tissues and organs was determined using regions of interest (ROIs) drawn over various organs such as the liver, lungs, brain, spleen, intestine and salivary glands. The activity was calculated from the ROI content in the whole-body scans using the conjugate view method. The activity estimations from the SPECT/CT images were made using ROIs drawn in each slice of the image volume and added as the number of counts in a volume of interest (VOI). Activity in organs,

blood and urine were calculated as percent of injected activity [%IA]. The %IA for the different organs, for urine and for blood are shown in Figure 19.

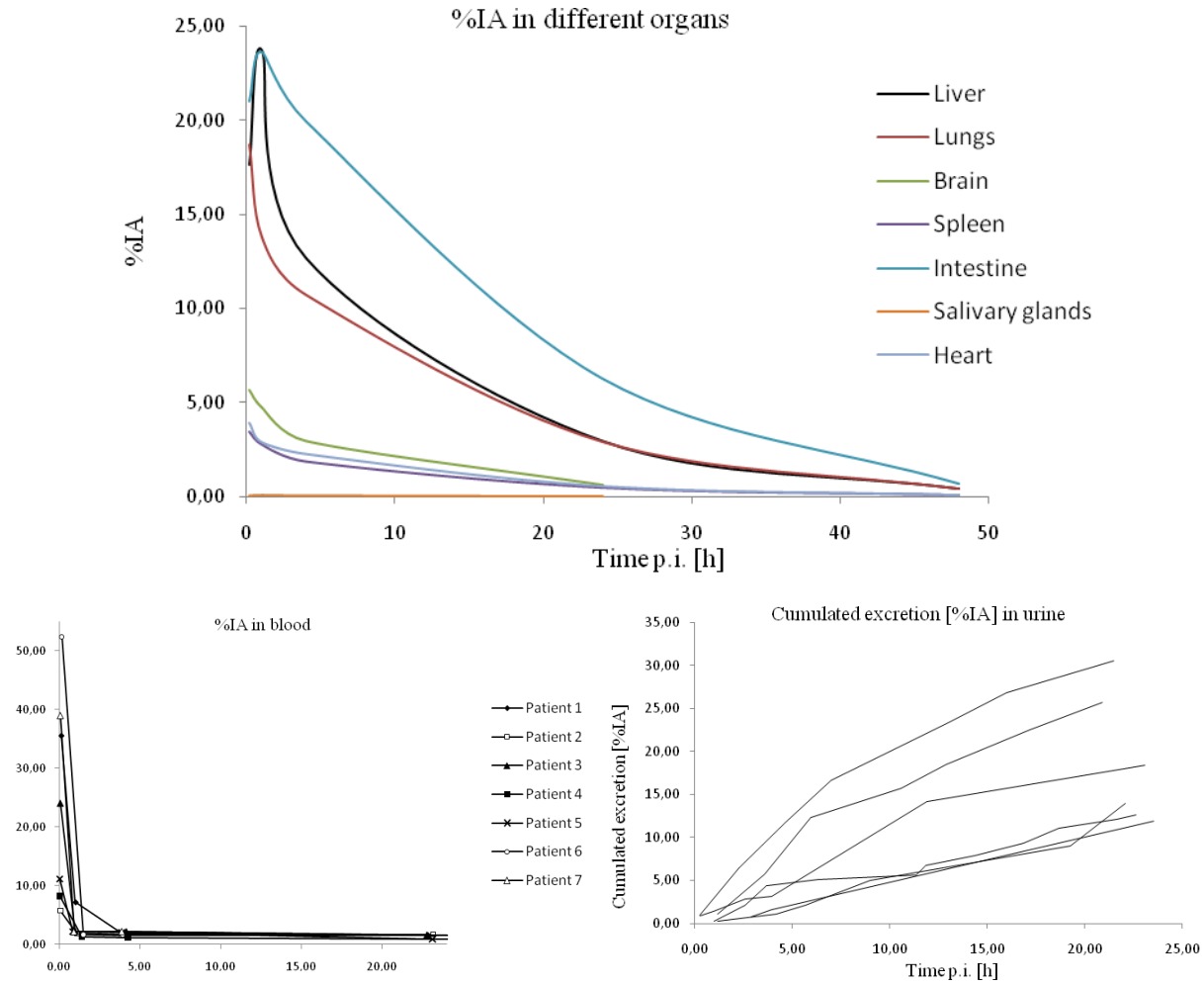

Figure 19. Estimated percentage of ^{123}I activity present in organs (upper panel), blood (lower left panel) and urine (lower right panel) at various time points after injection of ^{123}I-ioflupane.

The starting model was structured as follows: a central exchange compartment, where the radiopharmaceutical is initially administered, and a series of subsystems representing the organs which concentrated most of the activity and which were easily imaged in all patients: brain, lungs, liver, spleen and intestine. For only two patients activity concentrations were available also for the heart and the urinary bladder. Therefore the data of these two organs were not enough to consider them in the model. A further compartment (Rest of the Body, RoB) was added, in order to describe the material which is transported to organs and tissues different than those explicitly modeled. Identifiability of the compartmental model was verified using the GLOBI software. The model structure as obtained by the forcing function approach is shown in Figure 20.

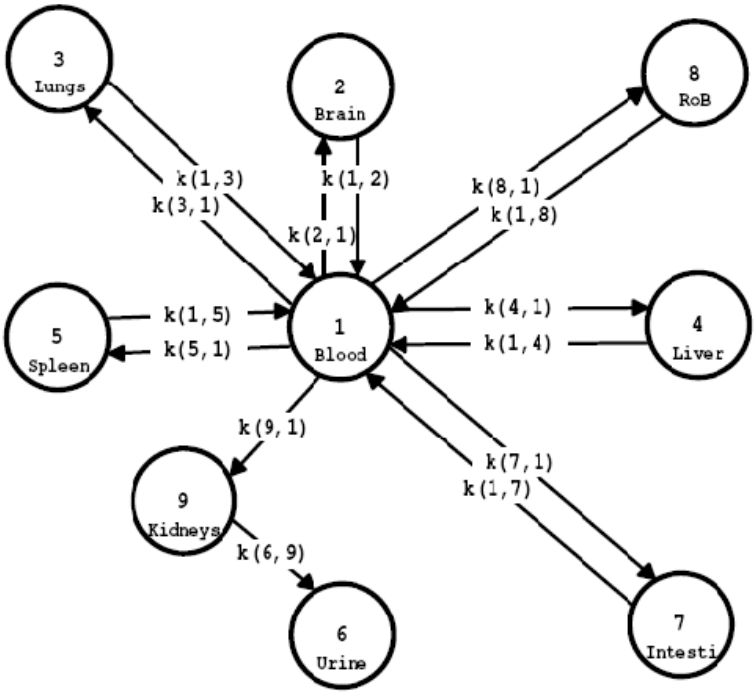

Figure 20. The compartmental structure resulting from the forcing function approach.
RoB: rest of the body.

The parameter values have been estimated using the software SAAM II Population Kinetics 1.0.1 with the Two Stage Iterative estimation method. Their values as obtained by the population fit of the model are shown in Table 2 together with the Population Standard Deviation (PSD).

Table 2. Values of the model parameters for ^{123}I-ioflupane biokinetics as obtained by the population fit of the model of Figure 3.13 to the available patient data.

Parameter	Mean [min^{-1}]	PSD [min^{-1}]	Parameter	Mean [min^{-1}]	PSD [min^{-1}]
Blood - Brain k(2,1)	$3.2\cdot10^{-2}$	$2.9\cdot10^{-2}$	Spleen - Blood k(1,5)	$8.2\cdot10^{-3}$	$3.2\cdot10^{-3}$
Brain - Blood k(1,2)	$1.38\cdot10^{-2}$	$0.44\cdot10^{-2}$	Blood - Intestine k(7,1)	$9.8\cdot10^{-2}$	$8.1\cdot10^{-2}$
Blood - Lungs k(3,1)	$2.0\cdot10^{-1}$	$2.3\cdot10^{-1}$	Intestine - Blood k(1,7)	$6.7\cdot10^{-3}$	$1.0\cdot10^{-3}$
Lungs - Blood k(1,3)	$1.00\cdot10^{-2}$	$0.45\cdot10^{-2}$	Blood - RoB k(8,1)	$1.64\cdot10^{-1}$	$0.91\cdot10^{-1}$
Blood - Liver k(4,1)	$5.58\cdot10^{-2}$	$0.48\cdot10^{-2}$	Rob-Blood k(1,8)	$7.1\cdot10^{-3}$	$6.8\cdot10^{-3}$
Liver - Blood k(1,4)	$7.6\cdot10^{-3}$	$4.2\cdot10^{-3}$	Blood - Kidneys k(9,1)	$7.9\cdot10^{-3}$	$9.4\cdot10^{-3}$
Blood - Spleen k(5,1)	$1.5\cdot10^{-2}$	$1.4\cdot10^{-2}$	Kidneys - Urine k (6,9)	$1.14\cdot10^{-2}$	$0.35\cdot10^{-2}$

Figure 21 shows for all the patients considered a good agreement of brain data to the model. More data would be useful to better validate the model considering that the first point of the plasma data, which is the most critical one for the model, presented a high variability within the six patients (average activity = 20.5%±15.2%), and also the total cumulated urinary excretion presented a high variability within the six patients (average activity = 10.4%±5.6%).

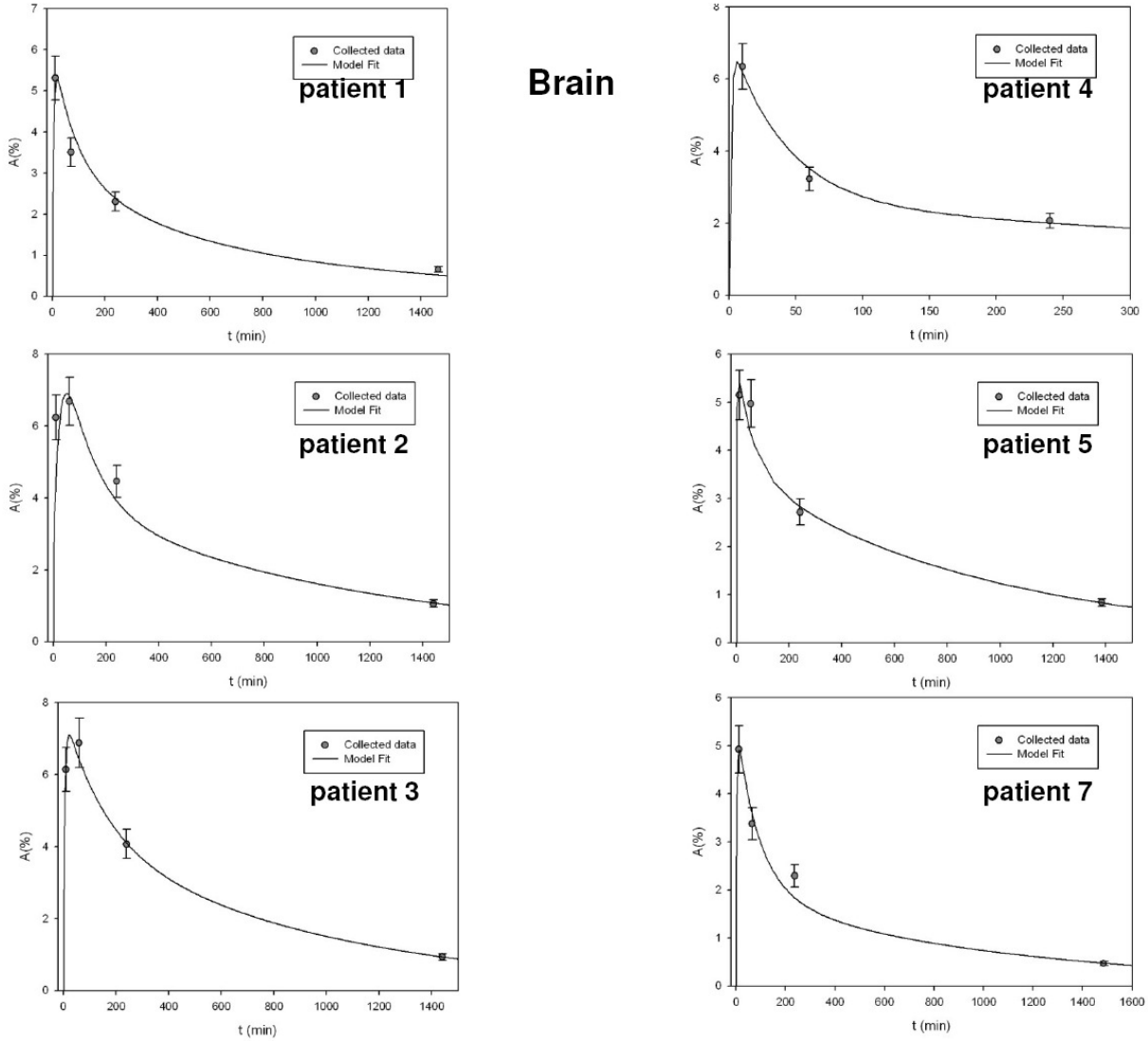

Figure 21. The individual prediction of the proposed model for the compartment brain compared with the patients' data as measured in WP1.

Development of optimal time scheme for patient data collection

As the main purpose of ^{18}F-choline examinations is the detection of tumors, metastases and recurrences (summarily addressed as lesions), optimization of the imaging procedure means optimizing the visibility of the lesions. Therefore we compared the activity concentrations in lesions and in several organs measured in the same PET scan for the three patients for whom lesions had been imaged.

The concentration ratios were normalized to the ratio at the first time point to visualize its time development. For the assessment we assumed that a higher ratio means a better contrast between lesion and organ. In liver and spleen the ratio kept a constant level around 1, because in these organs, as in the lesion, there is almost no biological clearance but only physical decay. For kidneys, the normalized ratio is systematically larger than 1 for t>1 h. This can be explained with the initial rapid decrease observed in the kidneys. Due to the magnitude of the associated uncertainties and the limited number of patients, however, the significancy of this trend was questionable. More evident was the increasing trend observed for the ratio lesion to bladder. In this case, there was a rapid uptake of the radiopharmaceutical into the bladder, shortly after the

administration, but the material was fully eliminated relatively frequently since the patients were asked to empty their bladder before the subsequent scan. This creates a favorable condition for the detection of the lesions in the region near or around the bladder, and additionally reduces the doses to this organ. To characterize this aspect further, use was made of the developed model structure. A simulation was performed, assuming fast uptake and infinite retention for the lesion, uptake into the bladder according to the results of the population model, and a voiding interval of 60 minutes. Figure 22 shows the ratio of the activity in the lesion to the activity in the bladder immediately before the voiding of the bladder, i.e. the worst possible case. The ratio at 5 minutes after administration was taken as the reference (normalization) ratio. Here again the ratio is increasing after 120 minutes. This ratio of lesion to bladder is especially interesting as the prostate is situated very close to the bladder. Therefore it is important but sometimes very hard for the radiologist to discriminate between activity in the bladder and uptake in a lesion. Our results are a first hint that at scans later than 60 minutes after administration a lesion in the vicinity of the bladder might be more visible even if the bladder had not been voided previous to the scan.

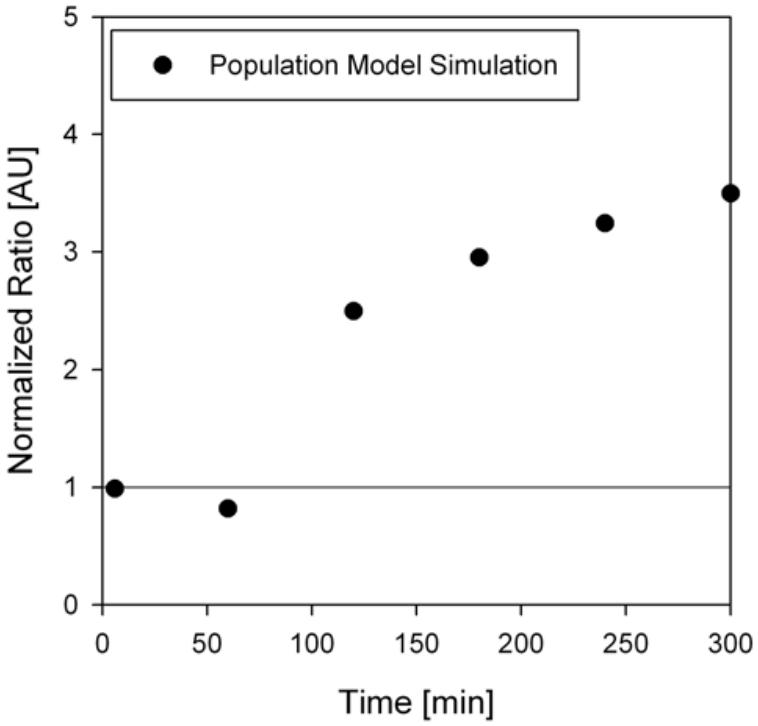

Figure 22. Simulated behavior of the ratio activity in lesion/activity in bladder.

Organ dose calculations using new ICRP reference voxel models

Preliminary sets of S-values for ^{18}F-choline and ^{123}I-iofluopane have been calculated. In the absence of biokinetic data, the S-values have been calculated for selected source regions where the radiopharmaceuticals are assumed to be distributed.

The tabulated values are based on monoenergetic Specific Absorbed Fractions (SAF) for photons and electrons. The SAF have been computed by the Monte Carlo method, where the particle transport has been performed by EGSnrc. The human body phantoms used for the SAF calculations are the adult male and female reference computational models that have been adopted by the ICRP and ICRU for their future dose calculations for radiation protection purposes. These reference computational phantoms have been developed in close cooperation with and supervision by the ICRP in order to cover several features important to external and internal dosimetry. In addition to the standard organs whose masses have been adjusted to the reference values of ICRP Publication 89, they contain, e.g., also lymphatic nodes and oral mucosa which are part of the remainder tissue

as defined in the ICRP 2007 Recommendations. Furthermore, their skeletons comply with ICRP Publications 70 and 89.
On the basis of these SAF-values the S-factors for ^{18}F-choline were calculated (see Deliverable 4.1) and combined with the time-integrated activity coefficients calculated using the biokinetic model of Figure 17. Table 3 gives the organ doses for selected target regions (a complete list of the doses to all target regions is given in the report associated to Deliverable 4.4).

Table 3 Time integrated activity coefficients and dose coefficients for the patients undergoing diagnostic studies with ^{18}F-choline

Organ	Time-integrated activity coefficients [h]		Organ	Dose coefficients [mGy/MBq]
Liver	0.422		Liver	0.062
Kidneys	0.114		Kidneys	0.079
Spleen	0.022		Spleen	0.038
Bladder contents	0.039		Bladder wall	0.017
Blood	0.270		Other tissues	≤ 0.031
Rest of the body	1.621			

A comparison between the dose values estimated using electron SAFs obtained from the adult male reference computational phantom, with explicit calculation of the electron absorption, and the dose values calculated according to the ICRP 30 approach, i.e., assuming that the electrons were locally absorbed, showed an agreement better than 6% for all non-source organs. As expected, the organ absorbed doses for the source organs evaluated with calculated electron SAFs were slightly lower than those for the ICRP 30 approach, with differences up to 5% for the solid source organs. The dose to the urinary bladder wall was found to be 38% lower when the calculated electron SAFs are used, compared to the ICRP 30 approach, due to large differences in the SAFs, especially at electron energies below 1 MeV.

Table 4 Time integrated activity coefficients and dose coefficients for the patients undergoing diagnostic studies with ^{123}I-ioflupane

Organ	Time-integrated activity coefficients [h]		Organ	Dose coefficients [mGy/MBq]
Liver	1.741		Liver	0.048
Kidneys	0.170		Kidneys	0.033
Spleen	0.437		Spleen	0.093
Brain	0.577		Brain	0.016
Lungs	4.864		Lungs	0.106
Intestine	3.422		Intestine	0.134
Blood	0.264		Bladder wall	0.019
Urinary bladder	0.173		Other tissues	≤0.030
Rest of the body	5.439			

Similarly the dose to patients undergoing investigations with ^{123}I-ioflupane was calculated using the biokinetic model presented in Figure 20, the model parameters presented in Table 2 and the S-

values for ^{123}I published in deliverable 4.1. The body regions where activity was accumulated (i.e., the source regions) were: blood, lungs, brain, kidneys, liver, intestine, and remaining tissues. Table 4 gives the time-integrated activity coefficients in the considered source regions and the dose coefficients for the most exposed organs. A complete list of doses to all target regions is given in the report associated to Deliverable 4.4.

Organ dose calculations using patient-specific voxel models

One patient-specific voxel phantom was segmented from the CT data of one of the patients recruited for the ^{18}F-choline study. The phantom was named MadPat (Madeira Patient). There are further individual voxel phantoms of adult male subjects available as members of the "HMGU voxel phantom family". Table 5 summarizes the main features of each of these phantoms, together with those of the adult male reference computational phantom. These phantoms were used to calculate monoenergetic photon and electron SAF values and the resulting S values for ^{18}F-choline. For each the patients the organ doses were estimated using the S-values calculated with the phantom that mostly resembled his own physical characteristic. Results are given in table 6.

Table 5 Physical characteristics of the computational phantoms

Phantom name	Reference Male	Frank	Golem	MadPat	Visible Human	Yale Man
Age (years)	na	48	38	69	38	na
Height (cm)	176	174	176	172	180	178
Weight (kg)	73	95	69	70	103	70
N. of voxel (millions)	1.95	23.7	1.9	8.3	20.1	1.0
Slice thickness (mm)	8	5	8	5	5	4
Voxel volume (mm^3)	36.5	2.7	34.6	6.9	4.3	56.3
Coverage	Whole body	Head and trunk	Whole body	Head to thigh	Head to thigh	Head to knee

Table 6 Individual time integrated activity coefficients and dose coefficients for the patients undergoing diagnostic studies with ^{18}F-choline

Biokinetic data – Time -integrated activity coefficients [h]										
Source organ	**1**	**2**	**3**	**4**	**5**	**6**	**7**	**8**	**9**	**10**
Liver	0.379	0.489	0.359	0.484	0.300	0.422	0.293	0.397	0.399	0.359
Kidneys	0.120	0.163	0.105	0.106	0.112	0.101	0.067	0.158	0.145	0.113
Spleen	0.027	0.014	0.020	0.034	0.018	0.034	0.028	0.013	0.008	0.021
UB contents	0.045	0.027	0.041	0.026	0.052	0.039	0.037	0.045	0.044	0.032
Blood	0.196	0.225	0.213	0.210	0.342	0.277	0.217	0.348	0.354	0.421
Rest of Body	1.723	1.609	1.749	1.680	1.611	1.616	1.866	1.503	1.519	1.558
Dosimetric data – Dose coefficients [mGy/MBq]										
Target region	**1**	**2**	**3**	**4**	**5**	**6**	**7**	**8**	**9**	**10**
Liver	0.071	0.090	0.053	0.062	0.041	0.056	0.041	0.061	0.061	0.056
Kidneys	0.067	0.088	0.072	0.053	0.062	0.051	0.037	0.105	0.097	0.080
Spleen	0.032	0.023	0.033	0.028	0.021	0.028	0.025	0.029	0.023	0.040
Bladder wall	0.039	0.028	0.017	0.017	0.027	0.018	0.019	0.017	0.017	0.015
Other tissues	≤0.028	≤0.033	≤0.028	≤0.030	≤0.022	≤0.028	≤0.024	≤0.031	≤0.031	≤0.030
Phantom used	MP	MP	RM	Frank	VH	Frank	Frank	RM	RM	RM

4. Potential impact and main dissemination activities

The approaches indicated here might enable to reduce the radiation exposure of the patients of at least a factor three to four. This will have a significant impact for the exposure of patients undergoing nuclear medical diagnostic procedures.

For example, in the diagnostic applications considered in this project, the patients received organ doses up to 40 mGy.

Table 3.5 Individual time integrated activity coefficients and dose coefficients for the patients undergoing diagnostic studies with ^{18}F-choline

Investigation	administered activity [MBq]	organs with highest doses	dose coefficient [mGy·MBq^{-1}]	dose [mGy]
^{18}F-choline	280-430	Kidneys	0.105	37*
		Liver	0.090	32*
^{123}I-Ioflupane	185	Intestine	0.134	25
		Lungs	0.106	20

*considering an administered activity of 350 MBq

With the introduction of the new techniques resulting from the MADEIRA research, it would be possible to reduce the organ doses down to maybe even below 10 mGy also for the most exposed regions. These massive dose reduction would result in a major benefit for the patients regarding the probability of secondary cancer induction assuming the linear-non-threshold theory as it is done in current international radiation protection approaches. In this case a four-fold reduction of secondary cancer in patients undergoing nuclear medical imaging procedures can be assumed not deteriorating image information. This is also a major potential social impact as costs due to cancer treatment can be avoided as the potential number of death due to ionizing radiation can be reduced. To do so, one major development was the introduction of new reconstruction tools which provide better signal-to-noise ratios in the images for less administered activity. Direct translation of such methods into the clinical market is foreseen since the SME partner of the project is the main contributor.

It is foreseen that the new reconstruction schemes, the new high spatial resolution hardware as well as the new biokinetic approaches need to be evaluated in various further clinical applications. The education program performed within the MADEIRA project will help to find young educated people taking care of such research opportunities and to bring the results quite fast into clinical practice together with the SME being a partner of MADEIRA as well as large medical imaging manufactures being cooperation partners of some of the participants.

4.1 Publications in peer reviewed scientific journals

The Consortium has published a total of 10 scientific manuscripts in international journals:

- Hoeschen et al.: Minimizing Activity and Dose with Enhanced Image quality by Radiopharmaceutical Administrations. Radiat. Prot. Dosim. 139 (2010), 250-3.
- Li and Hoeschen: Uncertainty and sensitivity analysis of biokinetic models for radiopharmaceuticals used in nuclear medicine. Radiat. Prot. Dosim. 139 (2010), 228-31.
- Linhart et al. Spectroscopy Study of Imaging Devices Based on Silicon Pixel Array Detector coupled to VATAGP7 Read-Out Chips. JINST (2011_JINST_6_C01092).

- Mattsson et al.: Medical imaging – optimisation in x-ray and molecular imaging. Rad Prot Dosim 139 (2010), 1-2.
- Mattsson and Söderberg: Radiation dose management in CT, SPECT/CT, and PET/CT techniques. Submitted to Rad Prot Dosim. (2010).
- Studen et al.: Timing performance of the silicon PET insert probe. Radiat. Prot. Dosim. 139 (2010), 199-203.
- Sydoff et al.: Absolute quantification of activity content from PET images using the Philips Gemini TF PET/CT system. Radiat. Prot. Dosim. 139 (2010), 236-9.
- Tischenko et al.: Main Features of the tomographic reconstruction algorithm OPED. Radiat. Prot. Dosim. 139 (2010), 204-7.
- Uusijärvi et al.: Biokinetics of ^{18}F-choline studied in four prostate cancer patients. Radiat. Prot. Dosim. 139 (2010), 240-4.
- Zankl et al.: New calculations for internal dosimetry of beta-emitting radiopharmaceuticals. Radiat. Prot. Dosim. 139 (2010), 245-9.

Some more manuscripts originating from the work performed in the frame of the project are currently under preparation and/or ready for submission:

- Giussani et al.: Training activities on radiation protection in nuclear medicine in the frame of the Euratom FP7 collaborative project MADEIRA. Submitted to Radiat. Measur.
- Giussani et al.: A population biokinetic and dosimetric model for ^{18}F-choline. In preparation
- Li et al.: Uncertainty analysis for ^{18}F-choline. In preparation
- Söderberg et al.: Optimisation and comparison of reconstruction algorithms (Flash 3D, ReSPECT, OPED). In preparation
- Studen et al.: The MADEIRA Pet probe. In preparation
- Sydoff et al: Biokinetics of ^{123}I-ioflupane. In preparation
- Tavola et al.: Non-linear compartmental model of ^{18}F-choline. To be submitted to Nucl. Med. Biol.
- Tavola et al.: A biokinetic model for ^{131}I-ioflupane. In preparation
- Uusijärvi-Lizana et al.: Biokinetics and dosimetry for ^{18}F-choline in prostate cancer patients. To be submitted to Eur. J. Nucl. Med.
- Zankl et al: Patient-specific SAF calculations. In preparation

4.2 Participation to national and international conferences

The Consortium has produced 24 presentations to international conferences and 4 presentations to national meetings related to the work performed in the frame of the project:

- Brzezinski et al.: *Monte-Carlo modelling of a silicon detector insert combined with a PET Scanner*. 5th European Molecular Imaging Meeting, Warsaw, Poland, May 26-29, 2010.
- Ebel and Engeland: *A new phantom for investigation of detectability in nuclear medicine tomography*. Course on "Quality assurance procedures for PET/CT and SPECT/CT", Malmö, Sweden, 24 June 2009.
- Facchinetti et al.: *Methods for the recovery of missing data in medical research*. LINSTAT 2010, Lisboa, Portugal, 27-31 July 2010.
- Giussani et al.: *A population kinetic model for ^{18}F-choline in prostate cancer patients*. Annual Congress of the European Association of Nuclear Medicine EANM, Wien, Austria, 9-13 October 2010.
- Hoeschen et al.: *Minimizing Activity and Dose with Enhanced Image quality by Radiopharmaceutical Administration (MADEIRA)*. Third Malmö Conference on Medical Imaging, Malmö, Sweden, 25-27 June 2009.

- Hoeschen et al.: *The progress in the MADEIRA project*. Third European IRPA Congress, Helsinki, Finland, 14-18 June 2010.
- Janzen et al.: *Preliminary compartmental model of ^{18}F-choline*. Third Malmö Conference on Medical Imaging, Malmö, Sweden, 25-27 June 2009.
- Janzen et al.: *Compartmental model of ^{18}F-choline*. SPIE Meeting, San Diego, USA, 13-18 February 2010.
- Li et al.: *Uncertainty of absorbed dose for radiopharmaceutical of ^{18}F-FDG*. SNM Annual Meeting, Toronto, Canada, 13-17 June 2009.
- Li and Hoeschen: *Uncertainty and sensitivity analysis of biokinetic models for radiopharmaceuticals*. Third Malmö Conference on Medical Imaging, Malmö, Sweden, 25-27 June 2009.
- Linhart et al.: *Development and test of TAB bonded silicon pad detectors and microcables for the construction of silicon probes for imaging devices*. 2009 NSS/MIC IEEE Conference, Orlando, Florida, 25 October- 1 November 2009. Conference Record, J05-10. P2423-2426, 2009.
- Linhart et al.: *Spectroscopy Study of Imaging Devices Based on Silicon Pixel Array Detector coupled to VATAGP7 Read-Out Chips*. IwoRID, Cambridge (UK), 11-15 July 2010.
- Linhart et al.: *Detection Tests of Imaging Devices Based on Silicon Pixel-Array Detectors Assembled Using Tape Automated Bonding and Microcable Technologies*. 2010 IEEE NSS MIC. 31 Oct-7 Nov 2010. Conference Record. M18-169.
- Mattsson et al.: *Radiation dose to patients from radiopharmaceuticals*. World Congress on Medical Physics and Biomedical Engineering, München, Germany, 7-12 September 2009.
- Stankova et al.: *Development and test of micro-cables for thin silicon detector modules in a prostate probe*. NSS/MIC IEEE conference, Dresden, Germany, 19-25 October 2008.
- Studen et al.: *Optimization of silicon detectors layout and associated front-end electronics for timing performance of a silicon PET through simulation*. NSS/MIC IEEE conference, Dresden, Germany, 19-25 October 2008.
- Studen et al.: *Timing performance of the silicon PET insert probe*. Third Malmö Conference on Medical Imaging, Malmö, Sweden, 25-27 June 2009.
- Studen et al.: *Timing in silicon PET probes*. Int.l symposium on advanced intraoperative imaging of radioisotopes, Mattinata, Italy, 4-6 September 2009.
- Studen et al.: *Performance of the MADEIRA PET probe prototype*. 2009 NSS/MIC IEEE Conference, Orlando, Florida, 25 October- 1 November 2009.
- Sydoff et al.: *Absolute quantification of activity content in PET images using the Philips Gemini TF PET/CT system*. Third Malmö Conference on Medical Imaging, Malmö, Sweden, 25-27 June 2009.
- Tavola et al.: *Il progetto europeo MADEIRA: le finalità del progetto***.** Proceedings of the Congress of the Italian Association for Radiation Protection, Pisa , Italy, 4-6 June 2008.
- Tavola et al.: *Compartmental model of ^{18}F-choline*. Congress of the Italian Association for Radiation Protection, Bolzano, Italy, 15-17 December 2010.
- Tischenko et al.: *Main features of data geometry required for the tomographic reconstruction algorithm OPED*. Third Malmö Conference on medical Imaging, Malmö, Sweden, 25-27 June 2009.
- Uusijärvi et al.: *Optimising PET/CT and SPECT/CT investigations. The MADEIRA project***.** Proceedings of the 6th international conference on Medical Physics in the Baltic States, Kaunas, Lithuania, 9-11 October, 2008.
- Uusijärvi et al.: *Biokinetics of ^{18}F-choline studied in four patients*. Third Malmö Conference on Medical Imaging, Malmö, Sweden, 25-27 June 2009.
- Uusijärvi et al.: *Biokinetics of ^{18}F-choline studied in four patients*. Swedish Medical Physicist Meeting, Uddevalla, Sweden, 17-18 September 2009.

- Uusijärvi-Lizana et al.: *Biokinetics and dosimetry for ^{18}F-choline in prostate cancer patients*. Malmö Cancer Center Research Retreat, Ven, Sweden, 26-27 August 2010.
- Zankl et al.: *New calculations for internal dosimetry of beta-emitting radiopharmaceuticals*. Third Malmö Conference on Medical Imaging, Malmö, Sweden, 25-27 June 2009.

Further participations to events in 2011 are planned:

- Giussani et al.: *Training activities on radiation protection in nuclear medicine in the frame of the Euratom FP7 collaborative project MADEIRA*. ORAMED Workshop, Barcelona, Spain, 20-22 January 2011.
- Li et al.: *Uncertainties of organ absorbed doses to patients from ^{18}F-choline*. SPIE Meeting, Orlando, USA, 12-17 February 2011.
- Mattsson et al.: *Current activities in the ICRP concerning estimation of radiation doses to patients from radiopharmaceuticals for diagnostic use.* International Conference on Image Optimisation in Nuclear Medicine, Ayia Napa, Cyprus, 23-26 March 2011.
- Söderberg et al.: *Initial tests of a new phantom for investigation of spatial resolution, partial volume effect and detectability in nuclear medicine tomography*. International Conference on Image Optimisation in Nuclear Medicine, Ayia Napa, Cyprus, 23-26 March 2011.
- Studen et al.: *MADEIRA Pet probe*, IEEE Nuclear Science Symposium and Medical Imaging Conference, Valencia, Spain, 23-29 October 2011,

4.3 Organization of scientific events

The MADEIRA Consortium has actively contributed to the organization of the 3rd Malmö Conference on Medical Imaging: Optimisation in X-Ray and Molecular Imaging, that was held in Malmö, Sweden, from 25 to 27 June 2009. Sören Mattsson from ULUND was chairing the Scientific Committee of the Workshop, and Christoph Hoeschen from HMGU was the Co-chair. They have also acted as guest editors for the Proceedings of the Conference, which were published in 2010 in the Journal Radiation Protection Dosimetry (Vol. 139).

4.4 Training courses

The organization of training courses, as well as the training of young scientists such as PhD students or Post-Doc researchers involved in the project, was part of the general goal to provide a specific education in the fields of physics and imaging applied to nuclear medicine.

With this view, a series of training courses was organized during the project, each covering a particular aspect of the research activities conducted by the Consortium.

The first MADEIRA Training Course on "Radiation Physics for Nuclear Medicine" was held in Milano from 18 to 21 November 2008, under the local organization of Università degli Studi di Milano and was dedicated to the memory of late Professor Niky Molho. During three and a half days, the course consisted in 16 lectures, including the keynote address by Professor Fridtjof Nüsslin (Nuklearmedizinische Klinik und Poliklinik, Klinikum rechts der Isar der Technischen Universität München, Munich, Germany), one session of guided exercises and a technical visit to the laboratory of the Joint Research Centre in Ispra. A total of 45 students originating from 16 countries (17 different nationalities, including also participants from non-European countries) attended the course. 27 applications for grants were received from 20 countries, 7 grants were assigned. Half of the lecturers were members of the MADEIRA Consortium, the remaining lecturers were experts coming from universities, international research centres and radiopharmaceutical industries. An evaluation form was distributed to the students at the end of the

course. The average overall rating was ranked at 4 on a scale going from 1 (bad) to 5 (excellent). Copies of the presentations in pdf-format were given to the students during the course.

The second MADEIRA Training Course on "Radiation Protection in Nuclear Medicine" was held in Malmö from 17 to 20 November 2009, under the local organization of Malmö University Hospital. During three and a half days, the course consisted in 14 lectures, two sessions of guided exercises and a technical visit to the nuclear medicine departments of the Malmö, Bispebjerg and Herlev Hospitals (the last two in Copenhagen, Denmark). A total of 44 students originating from 13 countries (13 different nationalities, including also participants from non-European countries) attended the course. 10 applications for grants were received, 7 grants were assigned. Lecturers were members of the MADEIRA Consortium and experts coming from universities, international research centers and clinical departments, including one lecturer working in the ORAMED project (a "sister" project funded within the frame of the EURATOM FP7). An evaluation form was distributed to the students at the end of the course. The average overall rating was ranked at 4 on a scale going from 1 (bad) to 5 (excellent). Copies of the presentations in pdf-format were made available to the students for download from the website of the course.

The third MADEIRA Training Course on "Imaging in Nuclear Medicine" was held in Munich from 5 to 8 October 2010, under the local organization of Helmholtz Zentrum München. During three and a half days, the course consisted in 16 lectures, two sessions of guided exercises and two technical visits (at the laboratories of Helmholtz Zentrum München and to the nuclear medicine department of Klinikum rechts der Isar in Munich). Also representatives from leading companies (Barco, IBA, and Siemens) were present at the event to inform the participants about career opportunities in the field of development of nuclear medicine technology and instruments. A total of 24 students originating from 9 countries (11 different nationalities, including also participants from outside Europe) attended the course. 12 applications for grants were received, 11 grants were assigned. Lecturers were members of the MADEIRA Consortium and experts coming from universities, international research centers and clinical departments. An evaluation form was distributed to the students at the end of the course. The average overall rating was ranked at 4.25 on a scale going from 1 (bad) to 5 (excellent). Copies of the presentations in pdf-format were made available to the students.

4.5 Other publications

An agreement was found with the publishing house Springer to publish a series of three books (MADEIRA book series) covering the topics of the MADEIRA Training Courses. The first volume ("Radiation Physics for Nuclear Medicine") has been issued in February 2011. The second and the third volumes ("Radiation Protection in Nuclear Medicine" and "Imaging in Nuclear Medicine") are planned to be published by mid 2012 at latest.

5. Address of project public website and relevant contact details

www.madeira-project.eu

www.madeira-training.org

Project coordinator

Prof. Dr. Christoph Hoeschen
Helmholtz Zentrum München – German Research Center for Environmental Health
Department of Medical Radiation Physics and Diagnostics
Ingolstäder Landstr. 1
85764 Neuherberg (Germany)
e-mail: christoph.hoeschen@helmholtz-muenchen.de

Project manager

Dr. Augusto Giussani
Helmholtz Zentrum München – German Research Center for Environmental Health
Department of Medical Radiation Physics and Diagnostics
Ingolstäder Landstr. 1
85764 Neuherberg (Germany)
Current address:
Federal Office for Radiation Protection
SG2.2 – Radiation and Health
Ingolstäder Landstr. 1
85764 Neuherberg (Germany)
e-mail: agiussani@bfs.de

Partner representatives

Prof. Sören Mattsson
Medical Radiation Physics, Lund University
Skåne University Hospital Malmö
SE-205 02 Malmö (Sweden)
e-mail: soren.mattsson@med.lu.se

Prof. Marko Mikuž
Institut Jozef Stefan
Jamova 39
1000 Ljubljana (Slovenia)
e-mail: marko.mikuz@ijs.si

Dr. Carlos Lacasta Llácer
CSIC-IFIC
Edificio Institutos de Investigacion
P.O.Box 22085
E-46071 Valencia (Spain)
e-mail: carlos.lacasta@ific.uv.es

Dr. Gernot Ebel
Scivis wissenschaftliche Bildverarbeitung GmbH
Bertha-von-Suttner-Str. 5
37085 Göttingen (Germany)
e-mail: ebel@scivis.de

Prof. Marie Claire Cantone
Università degli Studi di Milano
Dipartimento di Fisica – Sezione di Fisica Medica
Via Celoria 16
20133 Milano (Italy)
e-mail: marie.cantone@unimi.it

Prof. Neal Clinthorne
University of Michigan
Department of Radiology, Division of Nuclear Medicine
Zina Pitcher Place 204
48109-0552 Ann Arbor, Michigan (USA)
e-mail: nclintho@umich.edu